Dynamic interaction and instability of two moving proximate masses on a beam on a Pasternak viscoelastic foundation

Zuzana Dimitrovová

Department of Civil Engineering, NOVA School of Science and Technology, NOVA University of Lisbon, Portugal

and

IDMEC, Instituto Superior Técnico, Universidade de Lisboa, Lisboa, Portugal

E-mail: zdim@fct.unl.pt

https://doi.org/10.1016/j.apm.2021.07.022

Keywords: moving mass; mass-induced frequency; semi-analytical solution; dynamic interaction; instability; contour integration.

Abstract

The study analyzes the dynamic interaction of proximate masses using a new form of semi-analytical results for the moving mass problem developed by the author. This paper presents the results for a particular case of two moving masses of equal value acted upon by constant forces of equal values. The interaction level was demonstrated to be substantially high, making it impossible to superimpose the results obtained for one mass unless the masses were located at a significantly large distance apart. In the undamped case, the onset of instability occurred at the critical velocity, as with one moving mass; however, the onset of instability could be shifted significantly into the subcritical velocity range in the damped case. The critical distance between the moving masses was determined as the value at which the exponential increase in the amplitudes was severe. The implementation of dimensionless parameters revealed that this distance was slightly dependent on the damping. Moreover, the limiting moving mass ratio for such unexpected instability was derived.

The results were validated by eigenmode expansion analysis on long finite beams, for which computational time savings were proposed by the rearrangement of the terms involved. Excellent agreement between the results was obtained, validating the new formulae. Furthermore, extension to more general cases and additional moving masses can easily be achieved.

1. Introduction

Numerous engineering fields, particularly those relating to road and rail transport, include studies on structures subjected to moving loads. The increasing demands on rail networks and EU directives to shift from road to rail transport systems have renewed the need for an improved understanding of the dynamic phenomena pertaining to train-to-ground interactions. Thus, moving load problems remain active areas of current investigations.

Advances in symbolic software and high-precision calculations with an adaptable number of digits have promoted interest in semi-analytical solutions offering the benefits of closed-form solutions, thereby providing rapid and highly accurate results that can be directly supplemented by sensitivity and parametric analyses. In addition, the presentation of results involving dimensionless parameters enables a general view of the physical phenomena for a wide range of input data involved in the problem. Moreover, these results can only be evaluated in areas under focus, without a full-time history.

The moving load problem is a fundamental problem in structural dynamics; however, in its traditionally used designation, it is unclear whether the inertial effects in the moving object are considered. Thus, the problem specification should clearly state whether moving forces or masses, or oscillators, are considered [1], which can make a fundamental difference in solution methods and undesirable effects that may appear.

The moving force problem is much simpler than that with moving masses. When the force moves at a constant velocity over a homogeneous structure, analytical solutions for finite and infinite beams on a Pasternak viscoelastic foundation are available. These are conveniently summarized, for example, in a monograph [2]. The superposition of results is possible when the structure exhibits linear properties, and the initial instant is not vital for the analysis. For constant velocity, a steady-state stage can readily be achieved. A major concern relates to the resonant behavior for identifying the critical velocity, while questions regarding instability are irrelevant. Therefore, many works have analyzed only the steady-state regime. Among the recent works on analytical solutions, [3-4] are notable.

The moving mass problem is complex because it is inherently nonlinear and does not allow for the superposition of results, typically exploited in moving force problems. By applying the eigenvalue expansion method to homogeneous finite beams, it can be demonstrated that the governing equations in modal space are coupled, thereby requiring a complementary numerical solution or simplifications to ensure an acceptable approximate solution. The moving mass problem was initially solved using finite beams as early as 1929 by Jeffcott [5], using the method of successive approximations. The first solution obtained by eigenfunction expansion was probably published in [6]. The authors considered an undamped, simply-supported Euler–Bernoulli beam;

however, they omitted the Coriolis and centrifugal forces in the analysis. In [7], the so-called modal elements were developed. Methods apart from the finite element method include the spectral element method, dynamic Green's function [8], and reproducing kernel particle method [9]. The extension of the modal expansion method to a Timoshenko beam was presented in [10], whereas other issues such as control and support excitation were considered in [11-12]. A further extension to the accelerating mass by modal expansion was conducted in 1996 [13], and subsequently using the spectral element method [14] and with the aid of a newly developed finite element [15]. Large deflections were analyzed using finite elements in [16], and the numerical part was solved by perturbation analysis in [17]. Nevertheless, as this research aims to present the results in an analytical form as far as possible, the present discussion on state-of-the-art focuses on works with an analytical basis in the solution method, implying that numerous works using the finite element method are not mentioned.

Fewer works have been published on infinite beams. A pioneering study on the moving mass problem was presented in [18], where integral transforms were exploited, although the inverse transform was computed numerically. Furthermore, several solutions using integral transforms moved directly to the steady-state regime, thereby removing the inertial effect in the moving object and hiding the possibility of instability [19]. Other works exploited the moving element method [20], dynamic Green's function, and other methods. A review can be found in [21].

Instability issues resulting from anomalous Doppler waves induced in the beam may occur while the inertial objects move on a finite structure, but in general, published works on instability issues have been dedicated to infinite structures. In [22-23], the instability conditions were determined by the D-composition method; however, the full deflection shapes of the beam were not presented. It was also assumed that the unsprung mass was in permanent contact with the beam. In [24-25], a nonlinear contact spring was implemented. The deflection shapes were determined numerically, and the instability was analyzed by the D-composition method. In [26], the foundation model was extended to a double beam.

Regarding a sequence of moving masses, a pioneering solution on finite beams was presented in [27-28]. Double Fourier transform in which the possibility of instability was hidden was implemented in [29]. Among recent works on multi-span beams, [30] can be mentioned. A sequence of moving oscillators on an infinite beam was dealt with in [31] using Green's function method and the D-composition method to determine the instability conditions. The D-composition method was also used in recent work [32]. Whereas a contact spring was used in [31], in [32], it was again assumed that the unsprung mass was in permanent contact with the beam. An infinite string was considered in [33], and a numerical solution based on the differential quadrature method was presented in [34], but the masses were stationary.

The problem of several moving masses on a uniform homogeneous structure requires further attention from an analytical perspective. It is crucial to determine the conditions under which superposition is possible and whether the dynamic interaction leads to faster instability than expected. This can be achieved by exploiting the new form of result presentation published by the author [35-37]. The new form of results also enables the evaluation of the severity of the unstable behavior, which is vital for mitigation measures.

The solution presented in this paper is *conceptually different* from that in [31-32] because the full vibration shapes are determined semi-analytically and not numerically, and the instability is identified directly from the so-called *mass-induced frequency*. This term highlights the difference from the natural system frequencies because the mass-induced frequency, or simply induced frequency, is induced by the mass movement, and therefore dependent on its velocity. The final results are presented using dimensionless parameters allowing a wide range of realistic scenarios to be covered. Unlike in [31], where only one specific case was presented, readers of this paper can obtain the solutions to different problems without requiring recalculations. As a new result, it is demonstrated that damping can act oppositely and can shift the onset of instability into the subcritical region. Moreover, the so-called *critical distance* between masses is derived as the distance for which the lowest value of the imaginary part of an induced frequency is achieved.

In [35], the new presentation of the semi-analytical solution was derived under the assumption of homogeneous initial conditions. In [36], the solution was extended to non-homogeneous initial conditions, and in [37], further details on the method and an analysis of moving one- or two-mass oscillators were presented.

In this study, the problem of two moving masses was solved on an infinite homogeneous beam on a homogeneous viscoelastic Pasternak foundation and validated on an equivalent, sufficiently long finite beam. The analysis is limited to the tight contact assumption, commonly used in several works, such as [22-23, 32]. Nevertheless, the possible loss of contact can be examined *a posteriori*. In actual situations relating to vehicle motion, the loss of contact generally originates from severe inhomogeneities in the supporting structure, which is not the case in the present analysis. The other limitation is the massless foundation, also used by several other researchers. However, the analysis of this work can be extended to account for the wave propagation in the foundation, following [38-39], which will be the subject of further research.

The complete evolution of the transversal vibrations resulting from proximate moving masses is presented, as in [35-37], as a sum of several terms designated as the: (i) steady-state; (ii) *unsteady harmonic*; and (iii) *truly transient* part. The reasoning for the truly transient part has been presented in detail in [37]. Such designations are introduced because of the following reason. The solution should traditionally be separated into the steady-state and transient parts. However, as proven in

[35-37], the transient part has one dominant harmonic contribution described by a closed-form formula and another insignificant part. The dominant harmonic part is determined by the induced frequencies and can be formulated using standard harmonic terms. This is the reason that it must be named differently. The remaining part to be distinguished is designated as the truly transient part. All three parts represent the complete solution. By summing the first and second parts, the *harmonic solution* is obtained because the steady-state solution is also a harmonic term with zero frequency. Although it can be argued that the transient vibrations analysis may not be important because these will be attenuated by damping, any non-homogeneity in the structure will cause transient effects; therefore, it is essential to study such solutions. Additionally, instability cannot be detected without such an analysis.

One primary conclusion of this study is that the external viscous damping can act differently than for one moving mass where such damping always shifts the onset of instability into the supercritical velocity range. With proximate masses, damping can act oppositely and shift the onset of instability significantly into the subcritical range. Dimensionless parameters enable the definition of the so-called critical distance between moving masses. Assuming that the masses are at the critical distance, it is possible to determine the limiting moving mass ratio for which the instability occurs in the subcritical velocity range as a function of the applied damping. In contrast to the damped case, the onset of instability occurs exactly at the critical velocity for one or more moving masses in the undamped case. Furthermore, the analysis of the unsteady harmonic part of the beam vibrations enables the definition of the safe distance between masses, for which it is possible to use result superposition. It should be noted that the critical velocity and the velocity below which instability of the moving mass instability occurs are different factors. Instability velocities are not single velocities but constitute an interval, and the lowest one can be identified as the velocity at which the onset of instability occurs.

The rest of this paper is organized as follows: In Section 2, the problem under consideration is formulated, and the simplifying assumptions are listed. The derivation of the new closed-form formula for proximate moving masses is presented in Section 3. Section 4 is dedicated to examples. In Section 4.1, the range of parameters analyzed is established, and the validation possibility by finite beams analysis is described, along with the rearrangement of the involved terms in the eigenmode expansion method, leading to significant time savings, as in [38, 40]. Examples are discussed in Section 4.2 for the undamped case and Section 4.3 for the damped case. This section analyzes the derivation of the critical distance between moving masses and the conditions that determine the onset of instability in the subcritical velocity region. Finally, the main conclusions of this study are summarized in Section 5.

2. Problem statement

Consider the uniform motion of two constant masses traversing a horizontal infinite homogeneous beam supported by a Pasternak viscoelastic homogeneous foundation. The moving masses are acted on by vertical forces with harmonic components. The objective of the analysis is to determine the evolution of the vertical beam vibrations starting from homogeneous initial conditions. These results will confirm the strong dynamic interaction between the moving inertial objects, and thus, the impossibility of result superposition unless the objects are sufficiently far apart. The assumptions and simplifications for this analysis are outlined as follows:

(i) The beam is prismatic and straight, and its material is homogeneous and isotropic.

(ii) The beam may be subjected to an axial force acting on its axis (considered positive when inducing compression).

(iii) The beam obeys the linear-elastic Euler–Bernoulli theory.

(iv) The vertical displacement of the beam is measured from the equilibrium deflection position caused by the beam weight.

(v) The moving masses are always in contact with the beam, and their horizontal positions are determined by their velocity. This means that the contact is assumed as tight; each mass displacement and the displacement of the corresponding beam position are the same at all times.

(vi) No friction acts at the contact point.

(vii) The load and vertical displacement are considered as positive downward.

(viii) As is usual in several applications, the acting force does not represent the moving mass weight.

For practical applications, the beam represents the primary structure on which a vehicle moves (rail track or road), and the underlaid structure is simplified by a Pasternak foundation model with viscous damping. The axial force relates to the constrained thermal expansion of the primary structure. The action of the vehicle is represented by the moving constant masses and associated vertical forces. The harmonic component of the acting forces can simulate the imperfections in the contact region. In rail applications, these imperfections are attributed to the rail corrugation, wheel wear, and discrete supports as sleepers in ballasted tracks. A model of the system is depicted in Figure 1.

The equation of motion for the unknown vertical displacement field $w(x,t)$ can be expressed as

$$EIw_{,xxxx}(x,t)+\left(N-k_p\right)w_{,xx}(x,t)+mw_{,tt}(x,t)+c_b w_{,t}(x,t)+kw(x,t)=p(x,t) \qquad (1)$$

where *EI*, *m*, and *N* represent respectively, the bending stiffness and mass per unit length of the beam, and the axial force acting on the beam axis, considered positive when inducing compression. Moreover, k, k_p, and c_b are the Winkler's and Pasternak's moduli, and the coefficient of external viscous damping, respectively. The derivatives are designated by the respective variables in subscripts, preceded by a comma. The Pasternak modulus, the effect of which is usually associated with a shear layer, as indicated in Figure 1, can also be assumed as a distributed rotational spring. It can be observed from Eq. (1) that the Pasternak modulus has the same effect as the tension axial force.

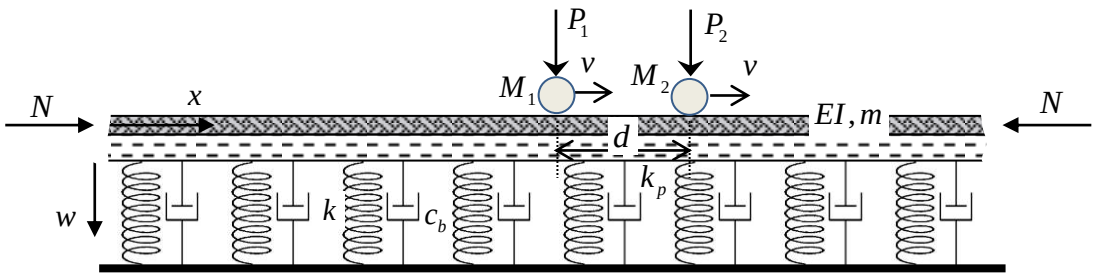

Figure 1: Infinite beam on viscoelastic Pasternak foundation subjected to axial force and two moving proximate masses acted on by vertical forces.

For two constant masses M_1 and M_2, and two associated forces P_1 and P_2 with constants P_{C_1} and P_{C_2} as well as harmonic components $P_{A_1}\sin\left(\omega_{f_1}t+\varphi_{f_1}\right)$ and $P_{A_2}\sin\left(\omega_{f_2}t+\varphi_{f_2}\right)$ moving at the same constant velocity *v*, the loading term $p(x,t)$ is expressed as

$$\begin{aligned} p(x,t) &= \left(P_{C_1}+P_{A_1}\mathrm{e}^{\mathrm{i}\left(\omega_{f_1}t+\varphi_{f_1}+3\pi/2\right)}-M_1 w_{01,tt}(t)\right)\delta(x-x_1) \\ &+\left(P_{C_2}+P_{A_2}\mathrm{e}^{\mathrm{i}\left(\omega_{f2}t+\varphi_{f2}+3\pi/2\right)}-M_2 w_{02,tt}(t)\right)\delta(x-x_2) \end{aligned} \tag{2}$$

where ω_{f_j}, $j=1,2$ are external excitation frequencies and φ_{f_j}, $j=1,2$ are phase angles. The exponential function is more convenient for the solution on an infinite beam, and therefore, a correction is introduced to the phase angle by $3\pi/2$ to match the sine function, which is preferable for analysis on finite beams. This addition is justified by the Euler formula, which results in $\mathrm{Re}\left(\mathrm{e}^{\mathrm{i}\left(\omega_{f_j}t+\varphi_{f_j}+3\pi/2\right)}\right)=\sin\left(\omega_{f_j}t+\varphi_{f_j}\right)$, $j=1,2$, but equally, $-\pi/2$ can be used, because $\mathrm{Re}\left(\mathrm{e}^{\mathrm{i}\left(\omega_{f_j}t+\varphi_{f_j}-\pi/2\right)}\right)=\sin\left(\omega_{f_j}t+\varphi_{f_j}\right)$, $j=1,2$. In the above, δ is the Dirac delta function and

$w_{0j}(t)$, $j=1,2$ are the mass displacements. The initial conditions are considered homogeneous. The boundary conditions state that the deflection and slope vanish for $x \to \pm\infty$.

3. Problem solution

To solve the problem defined by Eqs. (1) and (2) as well as the boundary and initial conditions, it is first necessary to remove the additional unknowns $w_{0j}(t)$, $j=1,2$ and express them in terms of the unknown deflection field $w(x,t)$. Owing to the assumption (v), $w_{0j}(t)=w(x_j,t)$, $j=1,2$ holds and $x_1=vt$, $x_2=vt+d$. Therefore, the relevant derivatives using the chain rule are:

$$w_{01,t}(t)=vw_{,x}(x,t)+w_{,t}(x,t) \text{ with } x=x_1 \tag{3}$$

$$w_{01,tt}(t)=v^2w_{,xx}(x,t)+2vw_{,xt}(x,t)+w_{,tt}(x,t) \text{ with } x=x_1 \tag{4}$$

$$w_{02,t}(t)=vw_{,x}(x,t)+w_{,t}(x,t) \text{ with } x=x_2 \tag{5}$$

$$w_{02,tt}(t)=v^2w_{,xx}(x,t)+2vw_{,xt}(x,t)+w_{,tt}(x,t) \text{ with } x=x_2 \tag{6}$$

Subsequently, the loading term reads as follows:

$$\begin{aligned}&\left(P_{C_1}+P_{A_1}\mathrm{e}^{\mathrm{i}\left(\omega_{f1}t+\varphi_{f1}+3\pi/2\right)}-M_1\left(w_{,tt}(x,t)+2vw_{,xt}(x,t)+v^2w_{,xx}(x,t)\right)\right)\delta(x-vt)\\&+\left(P_{C_2}+P_{A_2}\mathrm{e}^{\mathrm{i}\left(\omega_{f2}t+\varphi_{f2}+3\pi/2\right)}-M_2\left(w_{,tt}(x,t)+2vw_{,xt}(x,t)+v^2w_{,xx}(x,t)\right)\right)\delta(x-vt-d)\end{aligned} \tag{7}$$

and the equation of motion is updated to

$$\begin{aligned}&EIw_{,xxxx}(x,t)+\left(N-k_p\right)w_{,xx}(x,t)+mw_{,tt}(x,t)+c_bw_{,t}(x,t)+kw(x,t)\\&+M_1\delta(x-vt)\left(w_{,tt}(x,t)+2vw_{,xt}(x,t)+v^2w_{,xx}(x,t)\right)\\&+M_2\delta(x-vt-d)\left(w_{,tt}(x,t)+2vw_{,xt}(x,t)+v^2w_{,xx}(x,t)\right)\\&=\left(P_{C_1}+P_{A_1}\mathrm{e}^{\mathrm{i}\left(\omega_{f1}t+\varphi_{f1}+3\pi/2\right)}\right)\delta(x-vt)+\left(P_{C_2}+P_{A_2}\mathrm{e}^{\mathrm{i}\left(\omega_{f2}t+\varphi_{f2}+3\pi/2\right)}\right)\delta(x-vt-d)\end{aligned} \tag{8}$$

The three terms containing each moving mass have the following physical meanings—the mass inertial, Coriolis, and centrifugal force, respectively.

Following [35-37], it is convenient to introduce the moving coordinate $s=x-vt$, $t=t$. Thus, the governing equation in moving coordinates changes to

$$\begin{aligned}&EIw_{,ssss}+\left(N-k_p\right)w_{,ss}+m\left(w_{,tt}-2vw_{,st}+v^2w_{,ss}\right)+c_b\left(w_{,t}-vw_{,s}\right)+kw\\&=\left(P_{C_1}+P_{A_1}\mathrm{e}^{\mathrm{i}\left(\omega_{f1}t+\varphi_{f1}+3\pi/2\right)}-M_1w_{,tt}\right)\delta(s)+\left(P_{C_2}+P_{A_2}\mathrm{e}^{\mathrm{i}\left(\omega_{f2}t+\varphi_{f2}+3\pi/2\right)}-M_2w_{,tt}\right)\delta(s-d)\end{aligned}, \tag{9}$$

where the functional dependence on *s* and *t* is omitted for simplicity. The initial conditions are not affected by this change, as they are fixed at time *t*, and the boundary conditions state that the deflection and slope vanish for $s \to \pm\infty$. Several dimensionless parameters can be introduced to

simplify the resolution and analysis of the obtained results. These include the dimensionless spatial coordinate, time, and displacement, and frequency of the harmonic force

$$\xi = \chi s\,,\ \tau = \chi v_{cr} t\,,\ \widehat{w} = \frac{w}{w_{st}}\,,\ \widehat{\omega}_f = \frac{\omega_f}{\chi v_{cr}}\,, \tag{10}$$

where $w_{st} = \dfrac{P_{C_1}\chi}{2k}$ with $\chi = \sqrt[4]{\dfrac{k}{4EI}}$ is the maximum static displacement caused by the constant force P_{C_1} that is applied to the beam on Winkler's foundation k and $v_{cr} = \sqrt[4]{\dfrac{4kEI}{m^2}} = \dfrac{1}{\chi}\sqrt{\dfrac{k}{m}}$ is the critical velocity of a constant force that is moving uniformly on the beam on Winkler's foundation k. Further parameters are introduced for convenience:

$$\eta_b = \frac{c_b}{2\sqrt{mk}}\,,\ \eta_N = \frac{N}{N_{cr}} = \frac{N}{2\sqrt{kEI}}\,,\ \eta_S = \frac{k_p}{2\sqrt{kEI}}\,, \tag{11}$$

where N_{cr} represents the buckling critical force and η_b is conventionally referred to as the damping ratio, owing to the similarity with a one-degree-of-freedom oscillator. Indeed, the frequency of the specified infinite beam, independently of the Pasternak modulus and axial force, is $\omega_{\inf} = \sqrt{k/m}$, and thus, $c_{cr} = 2m\omega_{\inf} = 2\sqrt{mk}$ can be termed as the critical damping. It should be noted that the correct meaning of the critical damping corresponds to the damping level at which the separation between the evanescent and propagating waves occurs, which does not correspond to the previous value and strongly depends on the velocity and other parameters.

The final set of parameters relates to the moving load and its velocity:

$$\eta_{C_1} = \frac{P_{C_1}}{P_{C_1}}\,,\ \eta_{C_2} = \frac{P_{C_2}}{P_{C_1}}\,,\ \eta_{A_1} = \frac{P_{A_1}}{P_{C_1}}\,,\ \eta_{A_2} = \frac{P_{A_2}}{P_{C_1}}\,,\ \eta_{M_1} = \frac{M_1\chi}{m}\,,\ \eta_{M_2} = \frac{M_2\chi}{m} \text{ and } \alpha = \frac{v}{v_{cr}}\,. \tag{12}$$

Here, P_{C_1} is selected for measuring the relative values and normalizing the displacement. This selection is arbitrary and P_{C_2} can be selected in the same manner. In the particular case of moving harmonic forces; that is, when $P_{C_1} = P_{C_2} = 0$, either P_{A_1} or P_{A_2}, or some other convenient value must be used. Furthermore, η_{M_1} and η_{M_2} are known as the moving mass ratios and α can be referred to as the velocity ratio. In this definition, the classical value of the critical velocity is used, meaning that the critical resonance state occurs for $\alpha_{cr,ex} = \sqrt{1-\eta_N+\eta_S}$ under the influence of the axial force and the Pasternak modulus. Finally, the governing equation in the dimensionless form is expressed as

$$\begin{aligned}&\widehat{w}_{,\xi\xi\xi\xi}+4\left(\eta_N-\eta_S+\alpha^2\right)\widehat{w}_{,\xi\xi}+4\widehat{w}_{,\tau\tau}-8\alpha\widehat{w}_{,\xi\tau}+8\eta_b\left(\widehat{w}_{,\tau}-\alpha\widehat{w}_{,\xi}\right)+4\widehat{w}\\&=4\left(2\eta_{C_1}+2\eta_{A_1}\mathrm{e}^{\mathrm{i}\left(\bar{\omega}_{f1}\tau+\varphi_{f1}+3\pi/2\right)}-\eta_{M_1}\widehat{w}_{,\tau\tau}\right)\delta\left(\xi\right)\\&+4\left(2\eta_{C_2}+2\eta_{A_2}\mathrm{e}^{\mathrm{i}\left(\bar{\omega}_{f2}\tau+\varphi_{f2}+3\pi/2\right)}-\eta_{M_2}\widehat{w}_{,\tau\tau}\right)\delta\left(\xi-\widehat{d}\right)\end{aligned}\tag{13}$$

where $\widehat{d}$ is the dimensionless counterpart of the distance between masses, $\widehat{d}=\chi d$.

In the solution method, the Laplace transform

$$\tilde{F}\left(\xi,\bar{q}\right)=\int_0^\infty f\left(\xi,\tau\right)\mathrm{e}^{-\bar{q}\tau}\mathrm{d}\tau\ \text{ with }\ \bar{q}=\mathrm{i}q\tag{14}$$

is applied first, yielding the governing equation as

$$\begin{aligned}&\tilde{W}_{,\xi\xi\xi\xi}+4\left(\eta_N-\eta_S+\alpha^2\right)\tilde{W}_{,\xi\xi}-4q^2\tilde{W}-8\mathrm{i}q\alpha\tilde{W}_{,\xi}+8\left(\mathrm{i}q\eta_b\tilde{W}-\eta_b\alpha\tilde{W}_{,\xi}\right)+4\tilde{W}\\&=\left(\frac{8\eta_{C_1}}{\mathrm{i}q}+\frac{8\eta_{A_1}\mathrm{e}^{\mathrm{i}\left(\varphi_{f1}+3\pi/2\right)}}{\mathrm{i}q-\mathrm{i}\bar{\omega}_{f_1}}+4\eta_{M_1}q^2\tilde{W}\right)\delta\left(\xi\right)+\left(\frac{8\eta_{C_2}}{\mathrm{i}q}+\frac{8\eta_{A_2}\mathrm{e}^{\mathrm{i}\left(\varphi_{f2}+3\pi/2\right)}}{\mathrm{i}q-\mathrm{i}\bar{\omega}_{f_2}}+4\eta_{M_2}q^2\tilde{W}\right)\delta\left(\xi-\widehat{d}\right)\end{aligned}\tag{15}$$

Thereafter, the Fourier transform is applied:

$$F\left(p,\bar{q}\right)=\int_{-\infty}^{\infty}\tilde{F}\left(\xi,\bar{q}\right)\mathrm{e}^{-\mathrm{i}p\xi}\mathrm{d}\xi\tag{16}$$

which leads to

$$\begin{aligned}W\left(p,q\right)=\frac{1}{D\left(p,q\right)}\Bigg(&\frac{8\eta_{C_1}}{\mathrm{i}q}+\frac{8\eta_{A_1}\mathrm{e}^{\mathrm{i}\left(\varphi_{f1}+3\pi/2\right)}}{\mathrm{i}q-\mathrm{i}\bar{\omega}_{f_1}}+\frac{8\eta_{C_2}\mathrm{e}^{-\mathrm{i}p\widehat{d}}}{\mathrm{i}q}+\frac{8\eta_{A_2}\mathrm{e}^{\mathrm{i}\left(\varphi_{f2}+3\pi/2\right)}\mathrm{e}^{-\mathrm{i}p\widehat{d}}}{\mathrm{i}q-\mathrm{i}\bar{\omega}_{f_2}}\\&+4\eta_{M_1}q^2\tilde{W}\left(0,q\right)+4\eta_{M_2}q^2\tilde{W}\left(\widehat{d},q\right)\mathrm{e}^{-\mathrm{i}p\widehat{d}}\Bigg)\end{aligned}\tag{17}$$

where

$$D\left(p,q\right)=p^4-4p^2\left(\eta_N-\eta_S+\alpha^2\right)-4q^2+8\alpha pq+8\mathrm{i}\eta_b\left(q-\alpha p\right)+4\tag{18}$$

The inverse Fourier transform can now be applied to obtain the Laplace image of the displacement field

$$\tilde{F}\left(\xi,q\right)=\frac{1}{2\pi}\int_{-\infty}^{\infty}F\left(p,q\right)\mathrm{e}^{\mathrm{i}p\xi}\mathrm{d}p\tag{19}$$

$$\tilde{W}\left(\xi,q\right)=\frac{1}{\pi}\left(F_1+2\eta_{M_1}q^2\tilde{W}\left(0,q\right)\right)K\left(\xi,q\right)+\frac{1}{\pi}\left(F_2+2\eta_{M_2}q^2\tilde{W}\left(\widehat{d},q\right)\right)K\left(\xi-\widehat{d},q\right)\tag{20}$$

where

$$K\left(\xi,q\right)=\int_{-\infty}^{\infty}\frac{\mathrm{e}^{\mathrm{i}p\xi}}{D\left(p,q\right)}\mathrm{d}p\tag{21}$$

and

$$F_1=\frac{4\eta_{C_1}}{\mathrm{i}q}+\frac{4\eta_{A_1}\mathrm{e}^{\mathrm{i}\left(\varphi_{f1}+3\pi/2\right)}}{\mathrm{i}q-\mathrm{i}\bar{\omega}_{f_1}},\ F_2=\frac{4\eta_{C_2}}{\mathrm{i}q}+\frac{4\eta_{A_2}\mathrm{e}^{\mathrm{i}\left(\varphi_{f1}+3\pi/2\right)}}{\mathrm{i}q-\mathrm{i}\bar{\omega}_{f_2}}\tag{22}$$

$\tilde{W}(0,q)$ and $\tilde{W}\left(\hat{d},q\right)$ can be solved by substituting $\xi=0$ and $\xi=\hat{d}$ into Eq. (20):

$$\tilde{W}(0,q)\pi=\left(F_1+2\eta_{M_1}q^2\tilde{W}(0,q)\right)K(0,q)+\left(F_2+2\eta_{M_2}q^2\tilde{W}\left(\hat{d},q\right)\right)K\left(-\hat{d},q\right) \tag{23}$$

$$\tilde{W}\left(\hat{d},q\right)\pi=\left(F_1+2\eta_{M_1}q^2\tilde{W}(0,q)\right)K\left(\hat{d},q\right)+\left(F_2+2\eta_{M_2}q^2\tilde{W}\left(\hat{d},q\right)\right)K(0,q) \tag{24}$$

The previous equations can be written in the matrix form as follows:

$$\begin{bmatrix}\pi-2\eta_{M_1}q^2K(0,q) & -2\eta_{M_2}q^2K\left(-\hat{d},q\right)\\ -2\eta_{M_1}q^2K\left(\hat{d},q\right) & \pi-2\eta_{M_2}q^2K(0,q)\end{bmatrix}\cdot\begin{Bmatrix}\tilde{W}(0,q)\\ \tilde{W}\left(\hat{d},q\right)\end{Bmatrix}=\begin{Bmatrix}F_1K(0,q)+F_2K\left(-\hat{d},q\right)\\ F_1K\left(\hat{d},q\right)+F_2K(0,q)\end{Bmatrix} \tag{25}$$

It can be observed that the separate characteristic equations for each moving mass are placed on the diagonal of the main matrix. The determinant of this matrix identifies the characteristic equation of two moving masses:

$$\det=\left(\pi-2\eta_{M_1}q^2K(0,q)\right)\left(\pi-2\eta_{M_2}q^2K(0,q)\right)-4\eta_{M_1}\eta_{M_2}q^4K\left(\hat{d},q\right)K\left(-\hat{d},q\right) \tag{26}$$

which is reduced to the characteristic equation of $\eta_M=\eta_{M_1}+\eta_{M_2}$ for $\hat{d}=0$, as expected. Subsequently,

$$\tilde{W}(0,q)=\frac{\left(\pi-2\eta_{M_2}q^2K(0,q)\right)\left(F_1K(0,q)+F_2K\left(-\hat{d},q\right)\right)+2\eta_{M_2}q^2K\left(-\hat{d},q\right)\left(F_1K\left(\hat{d},q\right)+F_2K(0,q)\right)}{\det} \tag{27}$$

$$\tilde{W}\left(\hat{d},q\right)=\frac{\left(\pi-2\eta_{M_1}q^2K(0,q)\right)\left(F_1K\left(\hat{d},q\right)+F_2K(0,q)\right)+2\eta_{M_1}q^2K\left(\hat{d},q\right)\left(F_1K(0,q)+F_2K\left(-\hat{d},q\right)\right)}{\det} \tag{28}$$

Equations (27) and (28) can be substituted back into Eq. (20). Thus,

$$\begin{aligned}\tilde{W}(\xi,q)=&\frac{F_1\pi-2F_1\eta_{M_2}q^2K(0,q)+2F_2\eta_{M_1}q^2K\left(-\hat{d},q\right)}{\det}K(\xi,q)\\ &+\frac{F_2\pi-2F_2\eta_{M_1}q^2K(0,q)+2F_1\eta_{M_2}q^2K\left(\hat{d},q\right)}{\det}K\left(\xi-\hat{d},q\right)\end{aligned} \tag{29}$$

represents the analytical solution of the problem in the Fourier domain. In the special case of moving masses of the same value $\eta_M=\eta_{M_1}=\eta_{M_2}$, which are acted on only by constant forces also of the same value $\eta_C=\eta_{C_1}=\eta_{C_2}$, $\eta_{A_1}=\eta_{A_2}=0$, the previous expression can be simplified to

$$\begin{aligned}\tilde{W}(\xi,q)=&\frac{4\eta_C}{\mathrm{i}q}\frac{\pi-2\eta_Mq^2\left(K(0,q)-K\left(-\hat{d},q\right)\right)}{\det}K(\xi,q)\\ &+\frac{4\eta_C}{\mathrm{i}q}\frac{\pi-2\eta_Mq^2\left(K(0,q)-K\left(\hat{d},q\right)\right)}{\det}K\left(\xi-\hat{d},q\right)\end{aligned}. \tag{30}$$

Finally, the inverse Laplace transform can be performed. Starting with the definition

$$f(t)=\frac{1}{2\pi \mathrm{i}}\lim_{T\to\infty}\int_{a-\mathrm{i}T}^{a+\mathrm{i}T}F(s)\mathrm{e}^{st}\mathrm{d}s\,, \tag{31}$$

where *a* is a convenient positive number that ensures that all singularities are located to the right from the integration line, the expression reads as follows:

$$\widehat{w}(\xi,\tau)=\frac{1}{2\pi \mathrm{i}}\lim_{T\to\infty}\int_{a-\mathrm{i}T}^{a+\mathrm{i}T}\tilde{W}(\xi,\bar{q})\mathrm{e}^{\bar{q}\tau}\mathrm{d}\bar{q}=\frac{1}{2\pi}\int_{-\mathrm{i}a-\infty}^{-\mathrm{i}a+\infty}\tilde{W}(\xi,q)\mathrm{e}^{\mathrm{i}q\tau}\mathrm{d}q=\frac{1}{2\pi}I_{\tilde{W}_C}\,. \tag{32}$$

The integral $I_{\tilde{W}_C}$ in Eq. (32) can be evaluated by the contour integration method. A detailed analysis of the method's validity in the current case was presented in [37]. This analysis focuses on the definition of the region in the complex *q*-plane, where Cauchy's theorem can be used. It is determined that, for $\eta_b<1$, there is a limiting velocity α_C such that for $\alpha<\alpha_C$, two semi-infinite intervals $\langle -\infty+\mathrm{i}\eta_b,-q_{lm}+\mathrm{i}\eta_b\rangle$ and $\langle q_{lm}+\mathrm{i}\eta_b,+\infty+\mathrm{i}\eta_b\rangle$ exist, on which $K(\xi,q)$ is discontinuous for any ξ, because $D(p,q_r+\mathrm{i}\eta_b)$, which is understood as a polynomial expression for p, has real coefficients and the discriminant Δ of $D(p,q_{lm}+\mathrm{i}\eta_b)=0$ is zero. Moreover, q_{lm} is designated as the *limiting frequency*. Two branches are obtained by plotting q_{lm} as a function of α, but only the first branch for $\alpha\le\alpha_C$ can limit the semi-infinite intervals. When $\alpha\ge\alpha_C$, the discontinuity referenced above occurs along the full line $\langle -\infty+\mathrm{i}\eta_b,+\infty+\mathrm{i}\eta_b\rangle$. In general, no analytical expression exists for q_{lm}, but in the special case of $\eta_N=\eta_S$, which also includes the case when both parameters are null, a simple relation exists between q_{lm} and α for both branches:

$$\alpha_{1,\Delta=0}=\sqrt[4]{\frac{1}{8}\left(8+20q_{lm}^2-q_{lm}^4-q_{lm}\left(q_{lm}^2+8\right)^{3/2}\right)} \tag{33}$$

$$\alpha_{2,\Delta=0}=\sqrt[4]{\frac{1}{8}\left(8+20q_{lm}^2-q_{lm}^4+q_{lm}\left(q_{lm}^2+8\right)^{3/2}\right)} \tag{34}$$

This means that the integration contour must avoid the discontinuity lines through branch cuts. Further details can be found in [37]. Therefore, the integration along the branch cuts corresponds to the part of the final results that should be obtained numerically. It can be argued that, for $\alpha\ge\alpha_C$, it is more complicated to perform the integration along the branch cuts than directly performing the inverse Laplace transform numerically. However, this is not true because the integration along the branch cuts will contribute to the final results through a part with temporary importance, which is known as the truly transient vibration, and better numerical stability is achieved than when directly performing inverse Laplace transform numerically. The main role of the truly transient part is to adjust the initial conditions when the harmonic solution deviates from the initial values.

Furthermore, fully numerical results hide the individual harmonic terms essential for identifying the frequencies and amplitudes of the resulting vibrations, and thus, the stability.

The part that is obtained by the contour integration in Eq. (32), which is implemented for simplicity in Eq. (30) only, can be expressed as the sum of residues:

$$\begin{aligned}\widehat{w}\left(\xi,\tau\right)&=\sum\operatorname{res}\left(\frac{4\eta_C}{q}\frac{\pi-2\eta_{M_u}q^2\left(K\left(0,q\right)-K\left(-\widehat{d},q\right)\right)}{\det}K\left(\xi,q\right)\mathrm{e}^{\mathrm{i}q\tau},q\right)\\&+\sum\operatorname{res}\left(\frac{4\eta_C}{q}\frac{\pi-2\eta_{M_u}q^2\left(K\left(0,q\right)-K\left(\widehat{d},q\right)\right)}{\det}K\left(\xi-\widehat{d},q\right)\mathrm{e}^{\mathrm{i}q\tau},q\right)+\frac{1}{2\pi}I_{\tilde{W}_{bc}}\end{aligned}\tag{35}$$

where $I_{\tilde{W}_{bc}}$ represents the integration along the branch cuts. It can be observed that there exists one pole $q=0$ in both terms, which identifies the steady-state solution. Other poles can be obtained as roots of the characteristic equation $\det=0$. The number of roots of $\det=0$ is not known *a priori*, but it is carefully verified by the argument principle in all tested examples until $\alpha=1.4$ that this number is finite. For these roots, it is used to designate the mass-induced frequency, as outlined in Section 1. The objective of this paper is not to analyze the full range of velocities when the vibrations are highly unstable, and therefore, higher values of α are not considered.

Having determined the roots q_{M_j}, the harmonic terms from Eq. (35) can be obtained as follows:

$$\begin{aligned}\widehat{w}\left(\xi,\tau\right)&=\frac{4\eta_C}{\pi}K\left(\xi,0\right)+\sum_j 4\eta_C\frac{\pi-2\eta_{M_u}q_{M_j}^2\left(K\left(0,q_{M_j}\right)-K\left(-\widehat{d},q_{M_j}\right)\right)}{q_{M_j}\det{}_{,q}\left(q_{M_j}\right)}K\left(\xi,q_{M_j}\right)\mathrm{e}^{\mathrm{i}q_{M_j}\tau}\\&+\frac{4\eta_C}{\pi}K\left(\xi-\widehat{d},0\right)+\sum_j 4\eta_C\frac{\pi-2\eta_{M_u}q_{M_j}^2\left(K\left(0,q_{M_j}\right)-K\left(\widehat{d},q_{M_j}\right)\right)}{q_{M_j}\det{}_{,q}\left(q_{M_j}\right)}K\left(\xi-\widehat{d},q_{M_j}\right)\mathrm{e}^{\mathrm{i}q_{M_j}\tau}\end{aligned}\tag{36}$$

The terms in the sums identify the unsteady harmonic part of the solution. The roots can be determined by following the established methods in [35]. If the convergence of iterative methods from [35] is compromised, the argument principle may also significantly help. However, for appropriate use, it is vital to be aware of regions with discontinuities. Iterative methods can be programmed in MATLAB, but Maple can be used when high precision is required, or the critical results should be provided by Maple and passed to MATLAB. As with one moving mass, the roots always exist in pairs; that is, if q_{M_1} is a root, $q_{M_2}=\left(-q_{M_1}\right)^*$ is also a root (the asterisk designates the complex conjugate value). The condition $q_{M_2}=\left(-q_{M_1}\right)^*$ implies that such two frequencies always have the same imaginary parts and opposite real parts. The real parts form a harmonic function, whereas the imaginary parts indicate whether the related amplitude will gradually cease with time, become unstable (increase exponentially with time above all limits) or remain unchanged, which

will occur for the positive, negative, and zero imaginary values, respectively. Subsequently, the complex expressions can be transformed into classical forms with trigonometric functions because the amplitudes for each pair of frequencies are complex conjugates.

For further analysis, it is necessary to distinguish the unstable case (in which the vibration amplitude exponentially tends to infinity) from the subcritical, critical, and supercritical velocity cases, related to the comparison of the load velocity and critical velocity. It was demonstrated in [35, 37] that the unstable case for one moving mass always occurs at the critical velocity in the absence of damping and in the supercritical velocity range when damping is present. For this comparison, the extended formula for the critical velocity, which accounts for the axial force and Pasternak modulus, must be considered, namely $\alpha_{cr,ex} = \sqrt{1-\eta_N+\eta_S}$, as mentioned previously.

It will be demonstrated that this is not true for proximate masses. Dynamic interaction between the masses with damping can shift the onset of instability deep into the subcritical velocity range. The onset of instability is maintained at the critical velocity only in the undamped case, as for one moving mass. It should be noted that in the undamped case, $\alpha_{cr,ex} = \alpha_C$.

For one particular case, it is convenient to analyze the so-called *frequency lines*, which is the term for a curve where the induced frequencies are plotted as a function of α. Owing to the existence of discontinuities described in this section, the frequency lines are always cut when their imaginary part reaches the value of η_b. This implies that in the undamped case for $\alpha < \alpha_C$, when the imaginary part of the induced frequency is zero, the frequency line cannot cross the first branch of the limiting frequency q_{lm}. The number of frequencies is mainly dependent on α. For lower velocities in the subcritical velocity range, two pairs of induced frequencies exist, but this number is reduced to only one pair for higher velocity. The number of frequency pairs will increase again further from α_C. More details are provided in Sections 4.2 and 4.3. Nevertheless, in all cases examined until $\alpha = 1.4$, the maximum number of pairs is four. Thus, in all cases analyzed in this study, the sum in Eq. (36) is finite, and no additional approximation is required.

Full deflection shapes can be obtained aided by the adequate evaluation of $K(\cdot, q)$ with the dependence on ξ. This is a standard procedure, which again exploits the contour integration. For the wave ahead of the load, the positive contour in the upper complex *p*-half-plane is used, and for the rear wave, the negative value of the negative contour in the lower complex *p*-half-plane is used to fulfill the boundary conditions. Analytical expressions for the *p*-roots of $D(p, q)$ for a given q [37] can be exploited. The analysis of the nature of the roots is valid only for fourth-order polynomial expressions with real coefficients, but the formulae for the determination of the roots are general.

The other terms in Eq. (36) exhibit various forms of $K(g,q)$ and $K_{,q}(g,q)$ with $g=0,\hat{d},-\hat{d}$ for a given frequency. These expressions can also be evaluated precisely by contour integration. For example, if the roots with positive imaginary parts are designated as p_1 and p_2, for $g=0,\hat{d}$,

$$K(g,q)=\int_{-\infty}^{\infty}\frac{\mathrm{e}^{\mathrm{i}pg}}{D(p,q)}\mathrm{d}p=2\pi\mathrm{i}\sum_{j=1,2}\frac{\mathrm{e}^{\mathrm{i}pg}}{D_{,p}(p_j,q)} \tag{37}$$

which follows from the definition of the simple pole residue. Poles of the second order will always appear in the evaluation of

$$K_{,q}(g,q)=\int_{-\infty}^{\infty}\frac{-D_{,q}(p,q)}{D^2(p,q)}\mathrm{e}^{\mathrm{i}pg}\mathrm{d}p \tag{38}$$

because all roots of $D(p,q)$ are duplicated. Subsequently,

$$K_{,q}(g,q)=2\pi\mathrm{i}\sum_{j=1,2}\frac{-6\left(D_{,q}(p_j,q)\mathrm{e}^{\mathrm{i}gd}\right)_{,p}D^2_{,pp}(p_j,q)+2D_{,q}(p_j,q)\mathrm{e}^{\mathrm{i}gd}D^2_{,ppp}(p_j,q)}{3\left(D^2_{,pp}(p_j,q)\right)^2}. \tag{39}$$

As the induced frequencies are always located within the regions where $D(p,q)$ has four distinct complex roots, it is not necessary to analyze Eqs. (38) and (39) for exceptional cases.

4. Examples

4.1 Definition of case studies and validation

This section validates the new formulae in Eq. (36), examines the vibrations resulting from the dynamic interaction of two proximate masses, and analyzes the onset of instability. The importance of the truly transient part of the solution, that is, the option of neglecting it in the harmonic solution obtained by Eq. (36), is also discussed. Such an observation is important because it clarifies the possibility of using only the harmonic terms in closed-form analytical expressions that can be evaluated rapidly and accurately by suitable symbolic software. Moreover, owing to the nature of these formulae, the results do not lose precision with increasing time.

The validation of the new formulae is provided by carrying out analyses on long finite beams similar to those described in previous works [35-38]. Consistent with previous observations, simple supports are considered for the finite beams, owing to the simplicity of the vibration modes, analytical form of the wave-number, and numerical stability in the mode evaluation. To capture the initial instant correctly, the load on the finite beam must start to actuate slightly apart from the support, so as to remove its influence on the deflection shape that should be developed behind the load. As the foundation provides the primary support, the effect of the supports can be eliminated, and this fact was tested prior to presenting the results in [35]. The programs that calculate the beam response by the modal expansion method were written in MATLAB and were previously validated

by the commercial finite element software LS-DYNA. To approximate the deflection shape correctly, a relatively large number of modes must be considered, and convergence analysis on the number of modes was presented in [35]. The necessary number of modes also depends on the beam length; in general, at least 100 modes must be used for a dimensionless length of 50. For the presentation of the results, the beam length was determined with the value necessary to capture the dimensionless time interval considered for validation. In certain cases, 600 modes were necessary. To save computational time, the reordering of terms is proposed in the manner described below, similar to that in [38, 40].

Starting with Eqs. (1) and (2), the addition of boundary conditions for a simply supported beam and homogeneous initial conditions, and expanding over the undamped normalized vibration modes $w_j(x)$ as

$$w(x,t)=\sum_{j=1}^{\infty} q_j(t) w_j(x) \tag{40}$$

the equations (written in matrix form) for the determination of the modal coordinates $q_j(t)$ are obtained using standard techniques as follows:

$$\mathbf{M}(t)\cdot\mathbf{q}_{,tt}(t)+\mathbf{C}(t)\cdot\mathbf{q}_{,t}(t)+\mathbf{K}(t)\cdot\mathbf{q}(t)=\mathbf{p}(t) \tag{41}$$

It should be noted that Eq. (41) is coupled. If n vibration modes are considered, the square $n\times n$ time-dependent matrices $\mathbf{M}(t)$, $\mathbf{C}(t)$, and $\mathbf{K}(t)$ have terms that do not result from the discretization of the problem, as in the finite element method, but these terms are defined by the vibration modes in their exact analytical form, as follows:

$$M_{jk}(t)=\delta_{jk}+M_1 w_j(vt)\,w_k(vt)+M_2 w_j(vt+d)\,w_k(vt+d) \tag{42}$$

$$C_{jk}(t)=\delta_{jk}\frac{c_b}{m}+2M_1 v w_j(vt)\,w_{k,x}(vt)+2M_2 v w_j(vt+d)\,w_{k,x}(vt+d) \tag{43}$$

$$K_{jk}(t)=\delta_{jk}\omega_j^2+M_1 v^2 w_j(vt)\,w_{k,xx}(vt)+M_2 v^2 w_j(vt+d)\,w_{k,xx}(vt+d) \tag{44}$$

$$p_j(t)=\left(P_{C_1}+P_{A_1}\sin\left(\omega_{f_1}t+\varphi_{f_1}\right)\right)w_j(vt)+\left(P_{C_2}+P_{A_2}\sin\left(\omega_{f_2}t+\varphi_{f_2}\right)\right)w_j(vt+d), \tag{45}$$

where δ_{jk} is the Kronecker delta, $j,k=1,\ldots,n$, and the terms in the above equations are used only when the position vt or $vt+d$ falls with the beam region $\langle r,L\rangle$, respectively, where r represents the initial advance with respect to the left support. Thus, at zero time, the front mass is located at $r+d$, the rear mass at r, and the beam at rest because the intention is to validate the solution on infinite beams and not the sequential entrance of masses on a finite beam. It should be noted that matrices $\mathbf{C}(t)$ and $\mathbf{K}(t)$ are not symmetrical and that the axial force and Pasternak modulus only

affect the natural frequencies ω_j; that is, only the diagonal terms of the stiffness matrix. The axial force decreases the natural frequency, whereas the Pasternak modulus has the opposite effect.

As mentioned previously, a significant number of modes must be used. Therefore, similar to the case in [38], reordering is necessary. For $j,k=1,\ldots,n$,

$$M_{jk}=\delta_{jk} \tag{46}$$

$$C_{jk}=\delta_{jk}\frac{c_b}{m} \tag{47}$$

$$K_{jk}=\delta_{jk}\omega_j^2 \tag{48}$$

$$\tilde{\mathbf{M}}(t)=\begin{bmatrix} \left[M_{jk}\right] & -\left\{w_j(vt)\right\} & -\left\{w_j(vt+d)\right\} \\ \left\langle M_1 w_k(vt)\right\rangle & 1 & 0 \\ \left\langle M_2 w_k(vt+d)\right\rangle & 0 & 1 \end{bmatrix} \tag{49}$$

$$\tilde{\mathbf{C}}(t)=\begin{bmatrix} \left[C_{jk}\right] & \{0\} & \{0\} \\ \left\langle 2M_1 v w_{k,x}(vt)\right\rangle & 0 & 0 \\ \left\langle 2M_2 v w_{k,x}(vt+d)\right\rangle & 0 & 0 \end{bmatrix} \tag{50}$$

$$\tilde{\mathbf{K}}(t)=\begin{bmatrix} \left[K_{jk}\right] & \{0\} & \{0\} \\ \left\langle M_1 v^2 w_{k,xx}(vt)\right\rangle & 0 & 0 \\ \left\langle M_2 v^2 w_{k,xx}(vt+d)\right\rangle & 0 & 0 \end{bmatrix} \tag{51}$$

where $\left[\bullet,\bullet\right]$, $\{\bullet\}$, and $\langle\bullet\rangle$ denote matrices with dimensions of $n\times n$, $n\times 1$, and $1\times n$, respectively. This implies two additional full equations for two moving masses, but the main part of the matrix being diagonal has a dominant influence and leads to significant computational time savings for a high number of modes. Subsequently,

$$\tilde{\mathbf{M}}(t)\cdot\tilde{\mathbf{q}}_{,tt}(t)+\tilde{\mathbf{C}}(t)\cdot\tilde{\mathbf{q}}_{,t}(t)+\tilde{\mathbf{K}}(t)\cdot\tilde{\mathbf{q}}(t)=\tilde{\mathbf{p}}(t), \tag{52}$$

where

$$\tilde{\mathbf{q}}=\begin{Bmatrix} \{q_j\} \\ \lambda_1 \\ \lambda_2 \end{Bmatrix},\ \tilde{\mathbf{p}}=\begin{Bmatrix} \{0\} \\ P_{C_1}+P_{A_1}\sin\left(\omega_{f_1}t+\varphi_{f_1}\right) \\ P_{C_2}+P_{A_2}\sin\left(\omega_{f_2}t+\varphi_{f_2}\right) \end{Bmatrix}, \tag{53}$$

with λ_1 and λ_2 as additional variables, for which the following holds:

$$\begin{aligned} &\lambda_{1,tt}=P_{C_1}+P_{A_1}\sin\left(\omega_{f_1}t+\varphi_{f_1}\right) \\ &-\sum_k\left(M_1 w_k(vt)\,q_{k,tt}+2M_1 v w_{k,x}(vt)\,q_{k,t}+M_1 v^2 w_{k,xx}(vt)\,q_k\right) \end{aligned} \tag{54}$$

$$\lambda_{2,tt} = P_{C_2} + P_{A_2}\sin\left(\omega_{f_2}t + \varphi_{f_2}\right)$$
$$-\sum_k \left(M_2 w_k\left(vt+d\right)q_{k,tt} + 2M_2 v w_{k,x}\left(vt+d\right)q_{k,t} + M_2 v^2 w_{k,xx}\left(vt+d\right)q_k\right) \quad (55)$$

which designates the contact forces at each contact point.

All results obtained are presented in dimensionless form so that they can cover a wide range of parameter combinations. Therefore, the numerical input data presented later are not vital. The base values for the numerical data are motivated by railway applications, where the beam can be considered as the rail or as an equivalent beam representing the entire track. The case studies refer to one rail 60E1 supported by a viscoelastic Pasternak foundation with typical values, as in previous works.

Using the simplifications introduced in Section 3 in the form of $\eta_N = \eta_S = 0$ and $\eta_A = 0$, $\eta_C = 1$ can be assumed, and thus, all input data combinations are only dependent on α, $\widehat{d}$, η_M, and η_b. All parameters are assumed to cover realistic intervals of possible values. In particular, $\alpha = 0.01:0.01:1.4$ and $\eta_b = 0;0.04:0.01:0.99$ are considered, as these variations are supported by the physical meanings. Designations relating to the tested intervals follow the MATLAB convention—the first and last values define the minimum and maximum considered, whereas the middle value specifies the step between the consecutive values. This formalism will be used hereafter. Although very high values of η_b are obviously not realistic in practical applications, these values are important for the instability analysis, as explained later in Section 4.2. The other parameters are set to $\eta_M = 10:30:70$ and $\widehat{d} = 0.5:0.5:4.5$. For the sake of comparison, the case analyzed in [39] is described by $\chi = 0.445\text{m}^{-1}$, $\alpha = 0.344$, and $\eta_M = 74.1$. The tested distances range from $\widehat{d} = 1\chi = 0.455$ to $\widehat{d} = 10\chi = 4.45$.

Owing to space limitations, not all results covered by the ranges identified above are included in this paper. The graphs presented are mainly reduced to the deflection of the rear contact point for the sake of clarity. Full deflection shapes could also be obtained, but several similar cases are available in previous works.

The main focus is on the unsteady harmonic part of the solution, covering the dynamic interaction between the proximate masses. For the sake of completeness, the complete and harmonic solutions are also presented in the Appendix. This comparison serves as the validation and accuracy analysis of the harmonic solution. A comparison with the solution obtained by result superposition is presented for both situations. Moreover, for very close moving masses, the results obtained by one doubled mass are also provided.

As demonstrated previously in other works, the importance of the truly transient vibrations is proportional to the deviation of the displacement and velocity of the harmonic solution at $\tau = 0$

from zero; that is, from the homogeneous initial conditions. It is revealed that the truly transient vibrations can be omitted in most cases. As demonstrated before, cases in which the truly transient vibrations are important cannot be unequivocally defined *a priori*; nevertheless, they are more significant for lower η_M and are generally located around α_C, which is supported by the fact that the frequency lines are often cut around this value. Another aggravating factor is the increasing distance between the moving masses up to a particular value.

4.2 Undamped cases

The undamped cases, that is, when $\eta_b = 0$, are essential to analyze as limiting cases when the unsteady harmonic part of the vibrations lasts without alteration. It is demonstrated that these vibrations can be harmful and cannot be replaced by resulting superposition unless the masses are at a significant distance from one another. This is an academic case because damping is always present, but any disturbance will cause transient vibrations, and their analysis is more apparent in the undamped case.

As mentioned previously, $\eta_M = 10:30:70$, $\hat{d} = 0.5:0.5:4.5$, and the velocity ratios are analyzed over $\alpha = 0.01:0.01:1.4$. The induced frequencies are depicted in Figure 2.

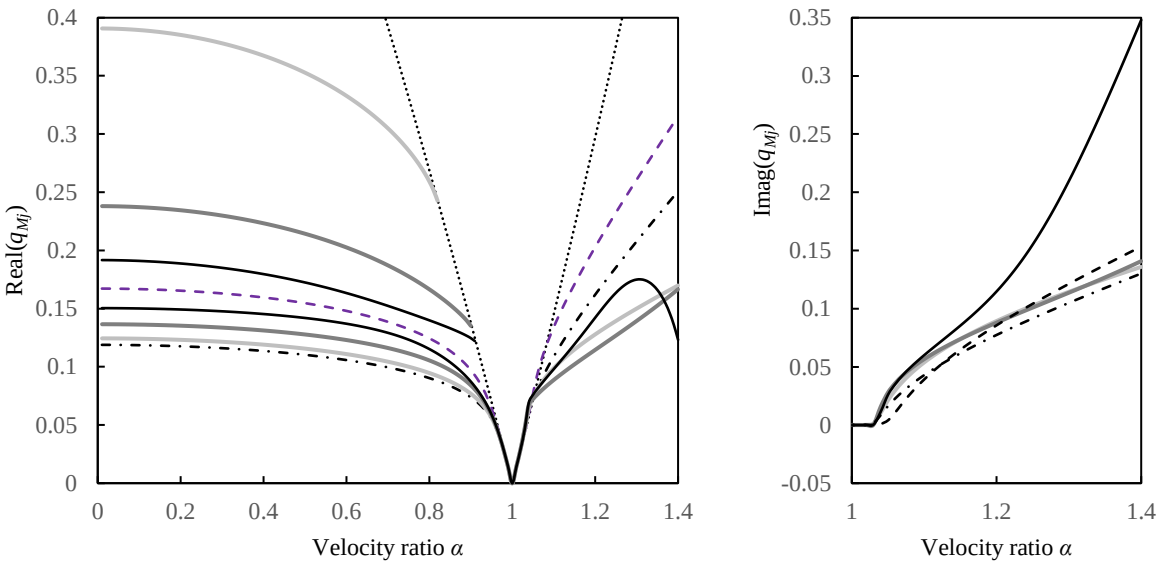

a)

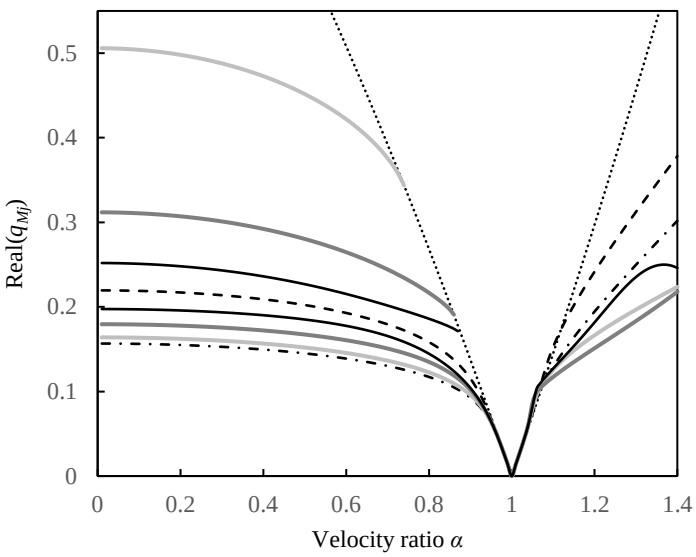
Real(q_{Mj})
0.5
0.4
0.3
0.2
0.1
0
0
0.2
0.4
0.6
0.8
1
1.2
1.4
Velocity ratio α

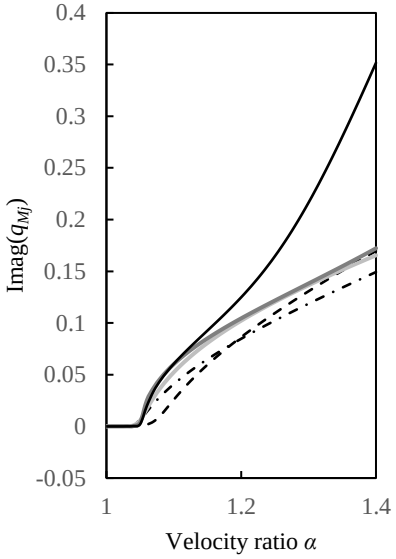
Imag(q_{Mj})
0.4
0.35
0.3
0.25
0.2
0.15
0.1
0.05
0
-0.05
1
1.2
1.4
Velocity ratio α

b)

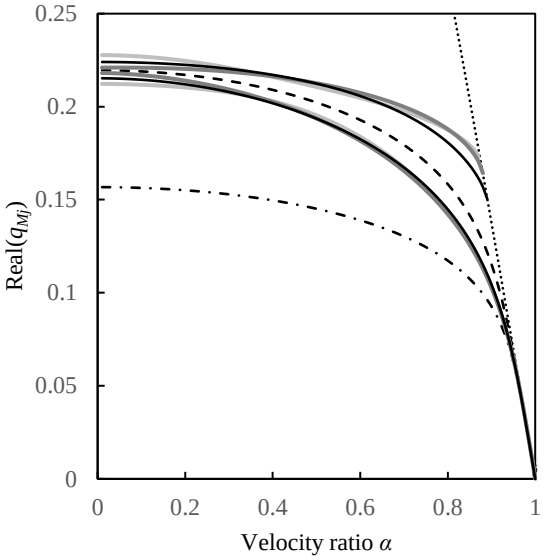
Real(q_{Mj})
0.25
0.2
0.15
0.1
0.05
0
0
0.2
0.4
0.6
0.8
1
Velocity ratio α

c)

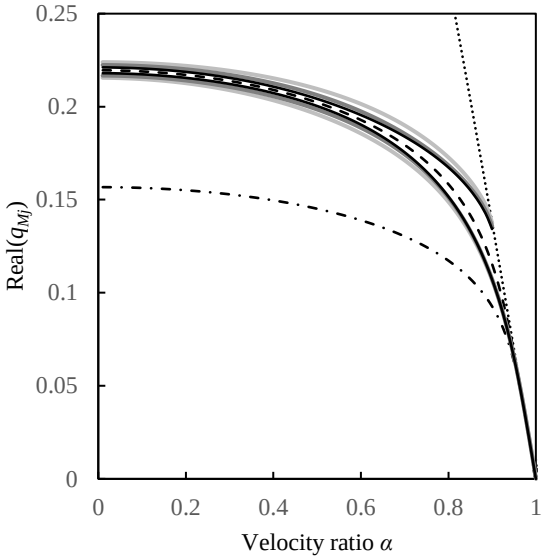
Real(q_{Mj})
0.25
0.2
0.15
0.1
0.05
0
0
0.2
0.4
0.6
0.8
1
Velocity ratio α

d)

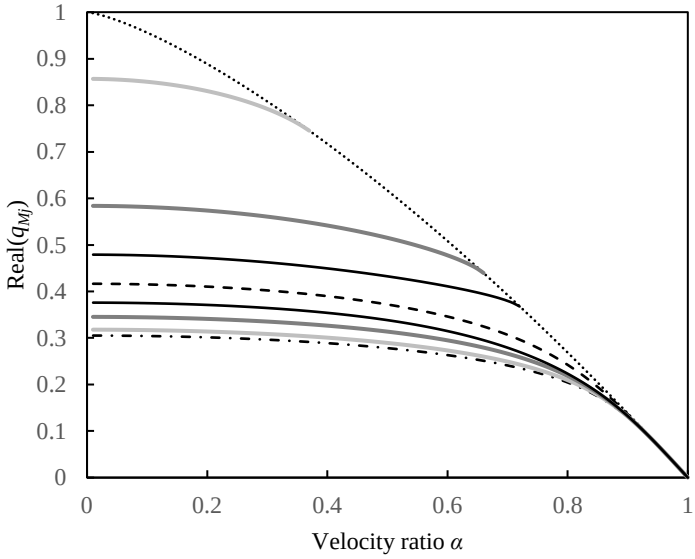
Real(q_{Mj})
1
0.9
0.8
0.7
0.6
0.5
0.4
0.3
0.2
0.1
0
0
0.2
0.4
0.6
0.8
1
Velocity ratio α

e)

Figure 2: Induced frequencies: a) $\eta_M = 70$, $\hat{d} = 0.5:0.5:1.5$; b) $\eta_M = 40$, $\hat{d} = 0.5:0.5:1.5$; c) $\eta_M = 40$, $\hat{d} = 2:0.5:4.5$; d) $\eta_M = 40$, $\hat{d} = 2:0.5:4.5$; e) $\eta_M = 10$, $\hat{d} = 0.5:0.5:1.5$ (black dotted – limiting frequency q_{lm}, black dashed – single mass, black dot-and-dash – doubled mass. The other lines are graded from light gray to black according to the increasing distance between masses).

For $\eta_M = 70$ and $\eta_M = 40$, the full velocity ratio range is shown for $\hat{d} = 0.5:0.5:1.5$. The real and imaginary parts of the induced frequencies are depicted separately. In the subcritical velocity range, the imaginary part is zero, and therefore, besides the frequency plotted in the graph, another one exists with the opposite value. In the supercritical velocity range, both parts are non-zero, and three other frequencies exist to cover all sign combinations. Thus, one of these has a negative imaginary part, indicating instability. This proves that the onset of instability starts precisely at the critical velocity. It should be noted that the imaginary part can be quite small, and thus, the exponential increase in the amplitudes is slow. Such values are hardly visible in Figures 2a) and b), but the onset is marked exactly at α_C, because for $\alpha > \alpha_C$, there is a discontinuity in the $K-$function along the real frequency axis, and therefore, the induced frequency cannot be real. Any complex induced frequency indicates the remaining other frequencies to complete the four sign combinations; thus, one of them will identify instability. The induced frequencies up to $\alpha = 1.4$ are shown only for $\hat{d} = 0.5:0.5:1.5$ and $\eta_M = 70$ or $\eta_M = 40$. In the other cases, the frequency lines are shown only in the subcritical velocity range because these values are used for the analysis of the dynamic interaction.

Regarding the frequencies in the subcritical velocity range, it can be observed that there are two pairs of frequencies for the lower α and only one for the higher α. For comparison, the frequencies relating to one single mass and one doubled mass are also included. It is clear that the lower frequency pair is always embedded between the limiting cases of the single and doubled masses. A smaller distance between the masses results in the frequency line being closer to that of the doubled mass, whereas a larger distance between the masses results in the frequency line being closer to that of the single mass. The higher frequency pair always lies outside this region, and the corresponding frequency line is cut by q_{lm}. Two general conclusions can be drawn: a lower η_M results in a lower α and a lower $\hat{d}$ in a lower α in the above situation. The first statement, which indicates that the lower frequency line is always embedded between the limit cases, supports the conclusion drawn in [39] that for a small distance between moving masses, the masses can be replaced by one doubled mass. However, it is demonstrated that this is not generally true. The

previous conclusion was misled by the constant relatively low $\alpha = 0.34$ and low time interval analyzed, and therefore, the additional changes in amplitudes that were imposed by the higher frequency were negligible.

Figures 3 to 6 focus on the unsteady harmonic solution. Function envelopes are included to highlight the amplitude variation. For clarity, only the vibration of the rear contact point as a function of τ is shown, as mentioned previously. The complete solution is provided in the Appendix. Three velocity ratios are selected: $\alpha = 0.5; 0.8; 0.9$. It is important to highlight that the steady-state solution is not included, and therefore, the upward displacements do not mean contact loss.

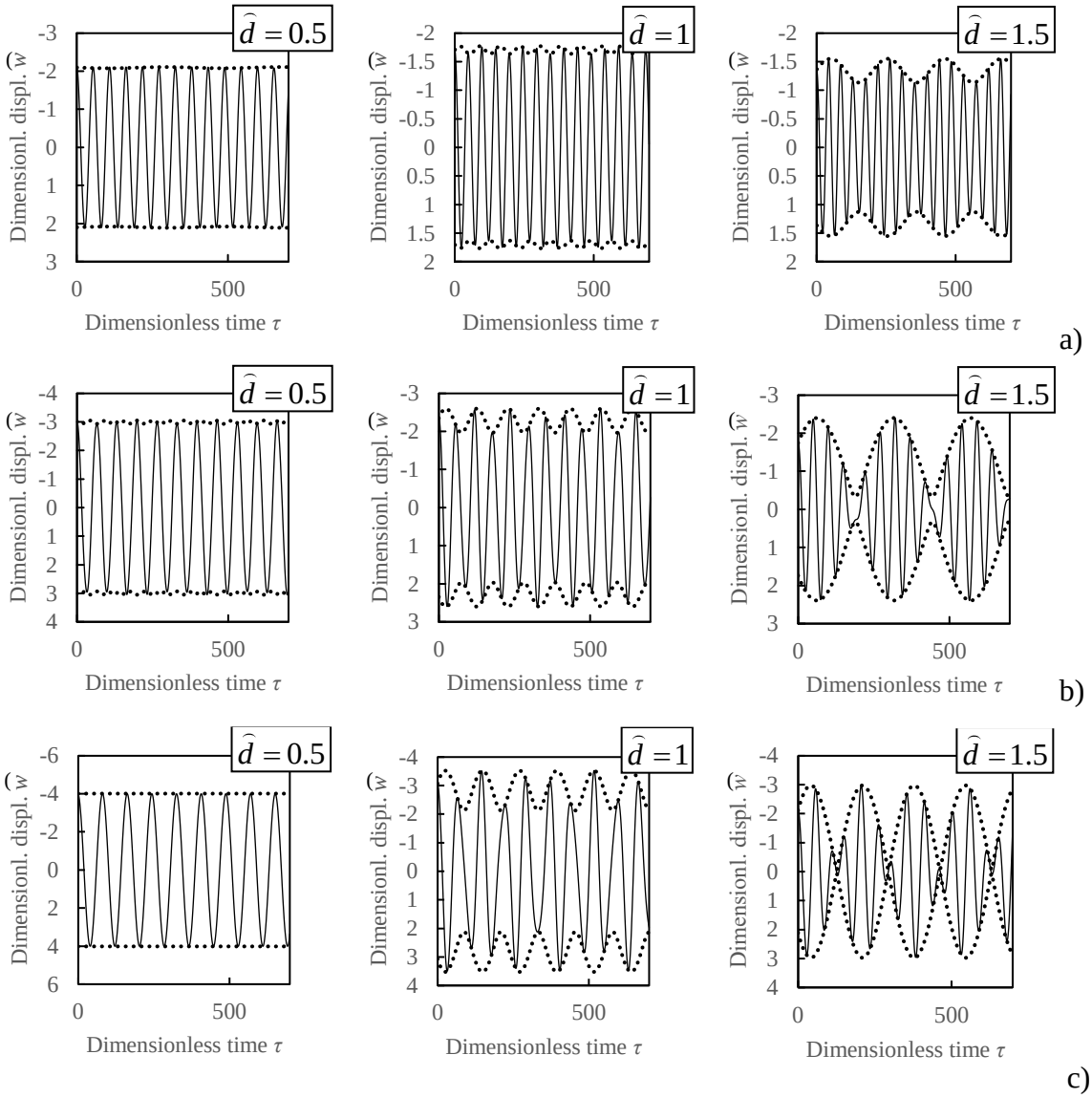

Figure 3: Unsteady harmonic part of vibrations for $\eta_M = 70$ and $\hat{d} = 0.5 : 0.5 : 1.5$: a) $\alpha = 0.5$; b) $\alpha = 0.8$; c) $\alpha = 0.9$ (black dotted lines indicate function envelopes).

It can be concluded from Figure 3 that by increasing $\hat{d}$ and α, the influence of the second induced frequency pair increases, and it is thus evident that result superposition would not be

possible because the amplitude remains unchanged in result superposition. Furthermore, for one doubled mass, there is no variation in the amplitudes. The above conclusion is not general because when the higher pair of frequencies is not present, the amplitudes are determined only from one pair and are consequently constant. This occurs for $\eta_M = 40$, where the higher frequency line is cut for a lower α; that is, the final α with both frequency pairs is $\alpha = 0.74; 0.86; 0.87$ for $\hat{d} = 0.5:0.5:1.5$, respectively. Moreover, $\eta_M = 40$ is tested further for larger distances, as reported in Figures 4 to 6.

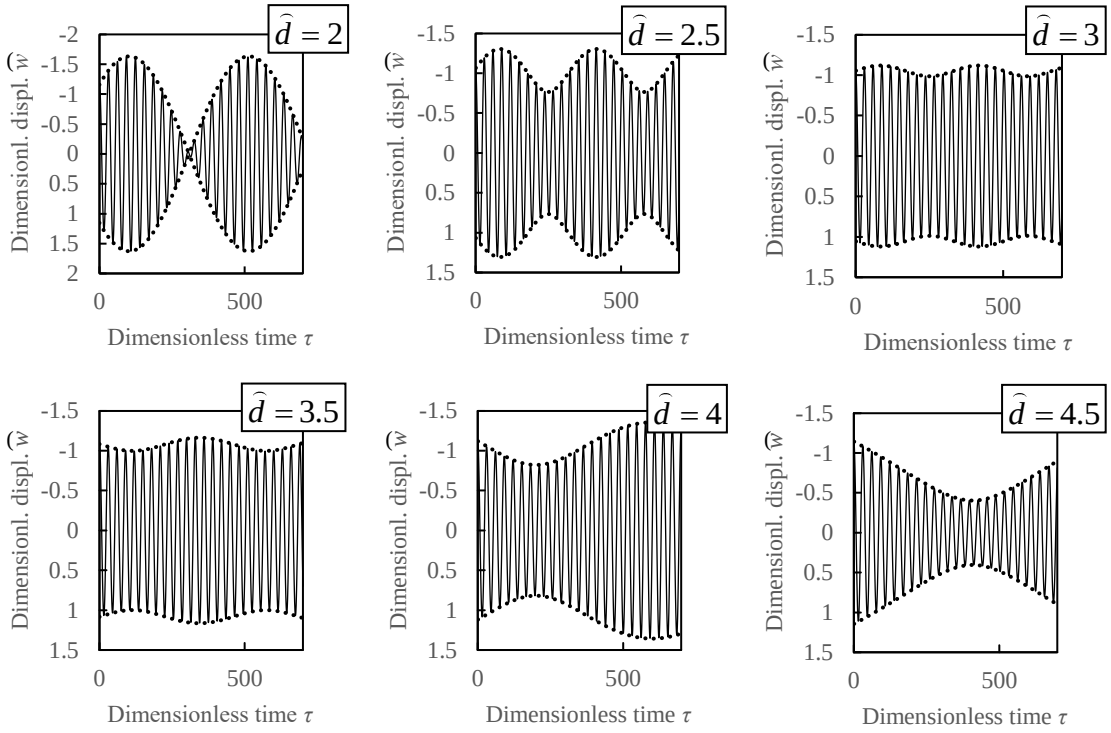

Figure 4: Unsteady harmonic part of vibrations for $\eta_M = 40$, $\alpha = 0.5$, and $\hat{d} = 2:0.5:4.5$ (black dotted lines indicate function envelopes).

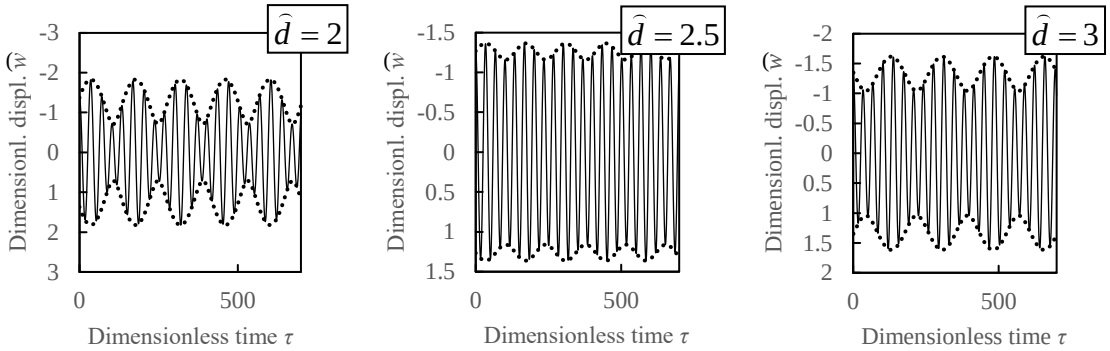

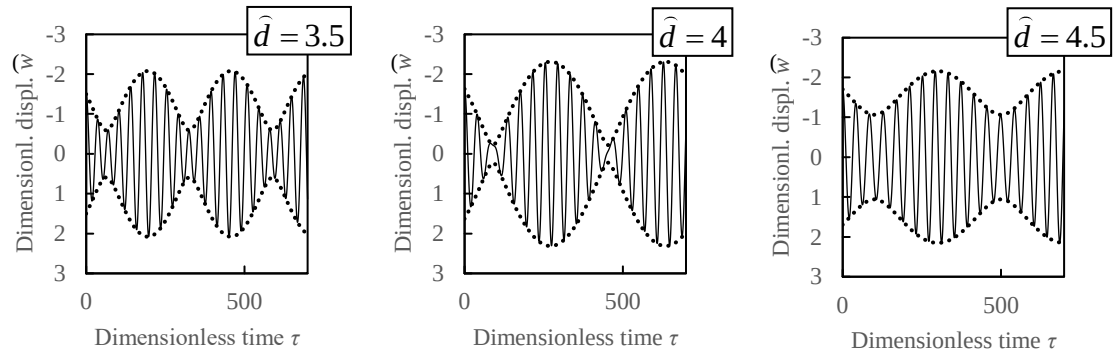

Figure 5: Unsteady harmonic part of vibrations for $\eta_M = 40$, $\alpha = 0.8$, and $\hat{d} = 2 : 0.5 : 4.5$ (black dotted lines indicate function envelopes).

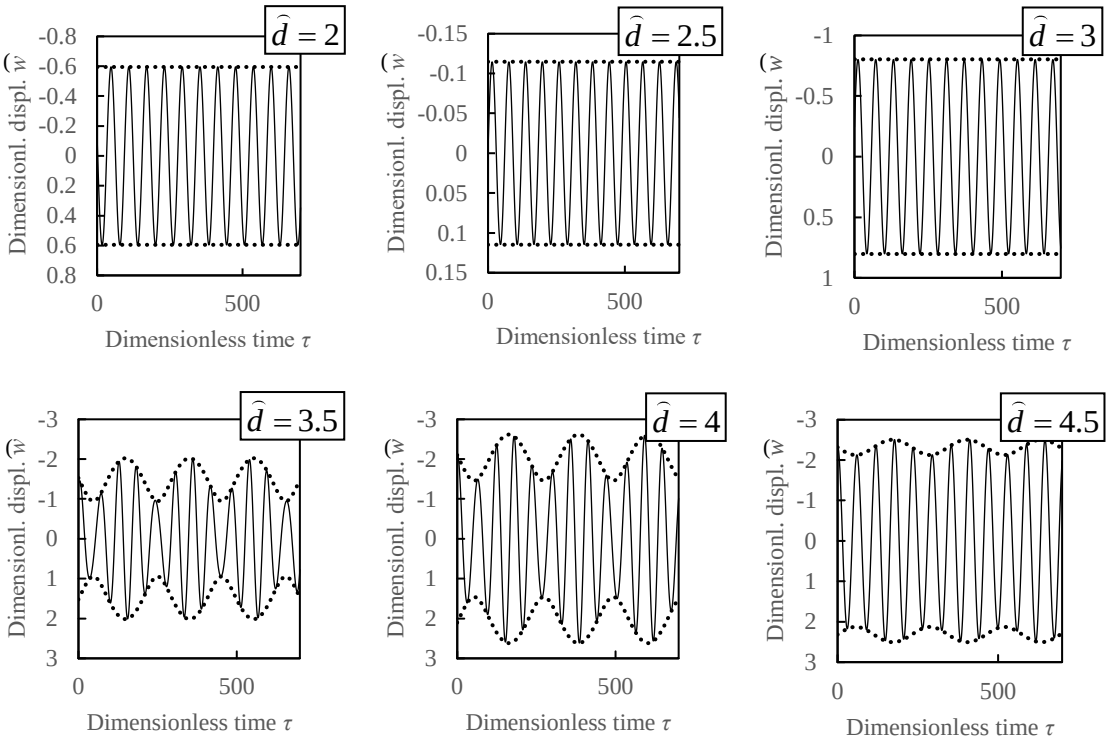

Figure 6: Unsteady harmonic part of vibrations for $\eta_M = 40$, $\alpha = 0.9$, and $\hat{d} = 2 : 0.5 : 4.5$ (black dotted lines indicate function envelopes).

The final α with both frequency pairs are $\alpha = 0.87; 0.88; 0.89; 0.90; 0.90; 0.90$ for $\hat{d} = 2 : 0.5 : 4.5$, respectively, and thus, the first three graphs in Figure 6 have constant amplitudes. Therefore, it can be concluded from Figures 4 to 6 that, even for $\hat{d} = 4.5$, the dynamic interaction between the two masses is not negligible, and result superposition cannot be used. Although several general statements can be deduced for the induced frequencies, very few general conclusions can be drawn regarding the dynamic interaction influencing the amplitude variation, as illustrated in Figure 7.

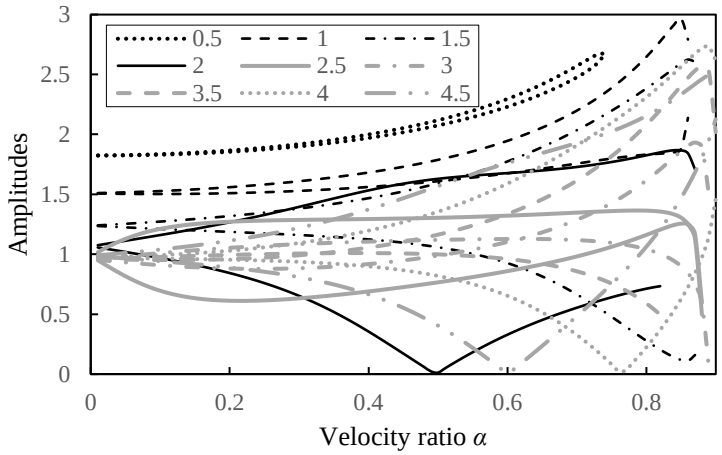

Figure 7: Maximum and minimum of function envelopes for $\eta_M = 40$ and $\hat{d} = 0.5:0.5:4.5$.

In Figure 7, the maximum and minimum of the function envelopes are plotted as a function of α for $\eta_M = 40$ and $\hat{d} = 0.5:0.5:4.5$. As there is no possible misinterpretation, for a fixed $\hat{d}$, both values use the same line code. Only the values when both frequency pairs exist are plotted. It can be concluded that there may exist α for which the minimum value is practically zero, but no general trend is observed.

For $\eta_M = 10$ and $\hat{d} = 0.5:0.5:1.5$, the final α values with both frequency pairs are only $\alpha = 0.37; 0.66; 0.72$ for $\hat{d} = 0.5:0.5:1.5$, respectively, and thus, only the case of $\alpha = 0.5$ is presented in Figure 8, with the final two graphs of variable amplitudes.

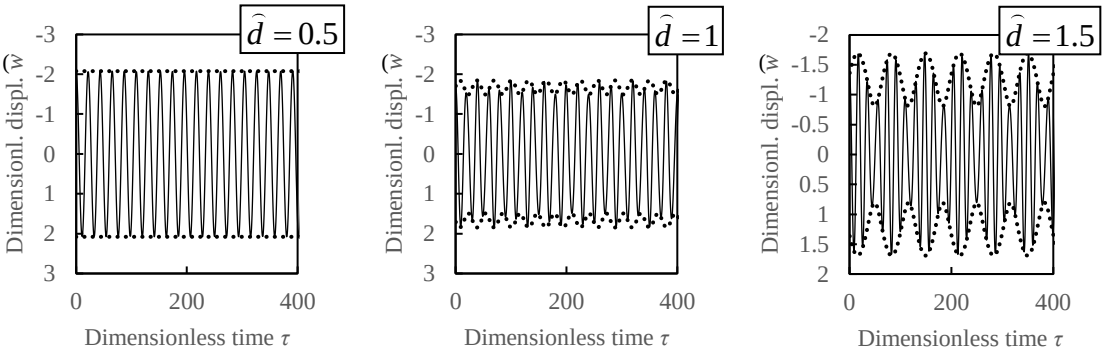

Figure 8: Unsteady harmonic part of vibrations for $\eta_M = 10$, $\hat{d} = 0.5:0.5:1.5$, and $\alpha = 0.5$.

4.3 Damped cases

In the damped cases, that is, when $\eta_b \neq 0$, the unsteady harmonic vibrations in the stable regime exponentially reduce the amplitudes, and they are negligible after a particular time. Thereafter, the full solution is completely described by its steady-state deflection. Thus, it appears that it is not important to conduct a detailed analysis after having thoroughly examined the undamped case.

However, this is not true because it is proven that damping can act in the opposite manner than that for one moving mass. It has been demonstrated in previous works that for one moving mass, a higher η_b results in a larger α for which the onset of instability occurs, and this always occurs only for $\alpha > \alpha_C$. It is proven that the dynamic interaction can shift the onset of instability deep into the subcritical range, a particularly dangerous effect. This cannot be detected from the steady-state solution or the undamped case. The induced frequencies are depicted in Figure 9, as in the undamped case.

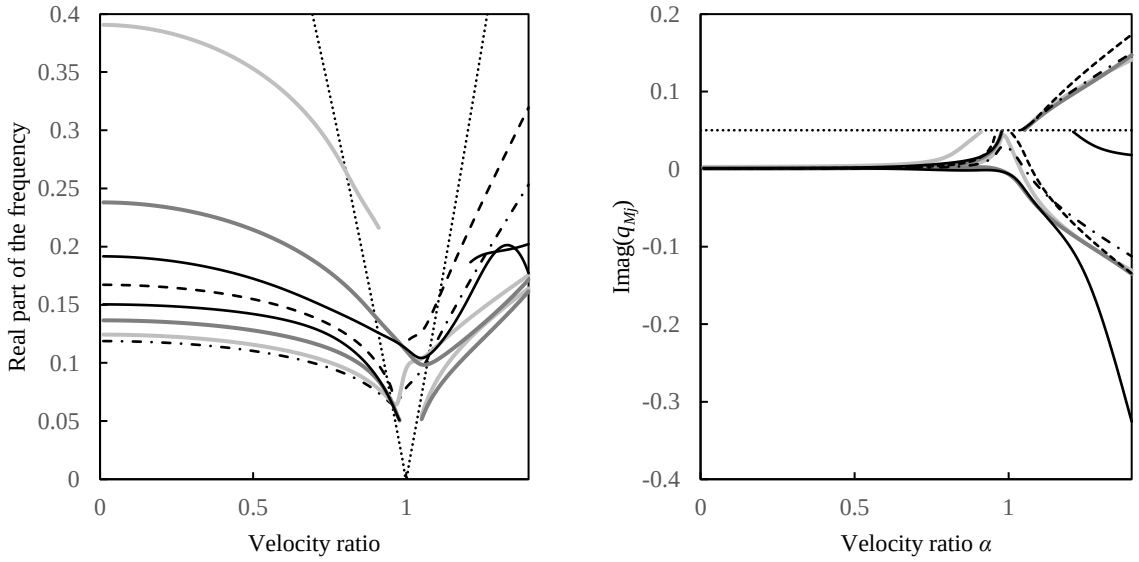

a)

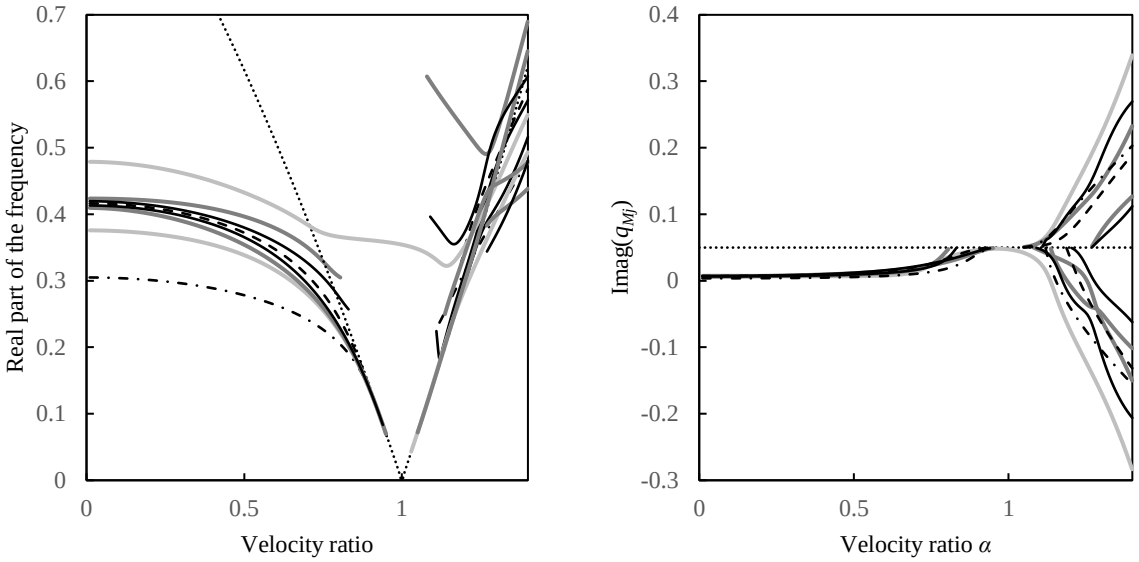

b)

Figure 9: Induced frequencies in damped case for $\eta_b = 0.05$: a) $\eta_M = 70$, $\widehat{d} = 0.5:0.5:1.5$; b) $\eta_M = 10$, $\widehat{d} = 1.5:1.5:4.5$ (black dotted – limiting frequency q_{lm} or interruption line at η_b-level, black dashed – single mass, black dot-and-dash – doubled mass. The other lines are graded from light gray to black according to the increasing distance between masses).

Figure 9 confirms that the frequency lines are cut when the imaginary part reaches the value of η_b. In contrast to the undamped case, the first branch of the limiting frequency q_{lm} can be crossed by the real part of the induced frequency because the imaginary part is always non-zero. In the damped case, there is no duplication, and each frequency that is plotted represents only one frequency pair. These statements are the same as those for one single mass. The difference is that the onset of instability occurs for $\alpha < \alpha_C$ when $\eta_M = 70$; that is, at $\alpha = 0.97$ and $\alpha = 0.67$ for $\hat{d} = 1$ and $\hat{d} = 1.5$, respectively.

By analyzing one particular subcritical velocity $\alpha = 0.99$ with $\eta_M = 70$ as a function of $\eta_b = 0.04 : 0.01 : 0.99$, it can be observed that the critical distance between the moving masses, defined as the distance for which the negative part of one of the induced frequencies is the lowest, is almost constant; it changes smoothly from 1.25 to 1.05 as the damping increases along the specified range. The evolution of the negative value is illustrated in Figure 10a). Furthermore, for several particular damping values, the limiting mass ratio for which the tested subcritical velocity $\alpha = 0.99$ already induces unstable behavior is depicted in Figure 10b). It should be noted that the induced frequencies for a fixed α as a function of η_M are more regular than the frequency lines where η_M is fixed and α varies.

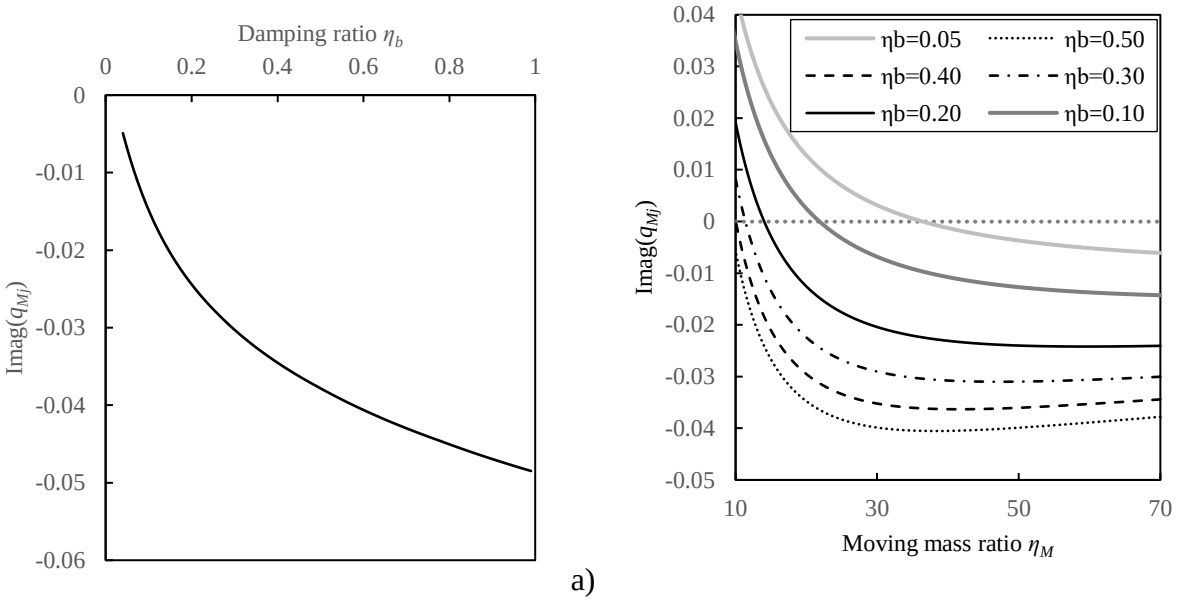

Figure 10: Lowest value of negative part of the induced frequency for fixed velocity $\alpha = 0.99$: a) for fixed $\eta_M = 70$ as function of η_b; b) as function of η_M for $\eta_b = 0.05; 0.1 : 0.1 : 0.5$ (dotted line indicates zero value).

It can be concluded from Figure 10 that if the moving masses are at the critical distance, instability occurs in the subcritical velocity range even for a relatively low η_M and typical η_b; e.g., $\eta_M = 21.9$ and $\eta_b = 0.1$.

Next, several analyses of the unsteady harmonic vibrations are presented. Only certain cases are selected for a fixed $\eta_b = 0.05$, namely $\eta_M = 70$ with $\widehat{d} = 0.5:0.5:1.5$ (Figure 11), because for $\eta_M = 10$ with $\widehat{d} = 1.5:1.5:4.5$, the unsteady part of the vibrations is rapidly damped.

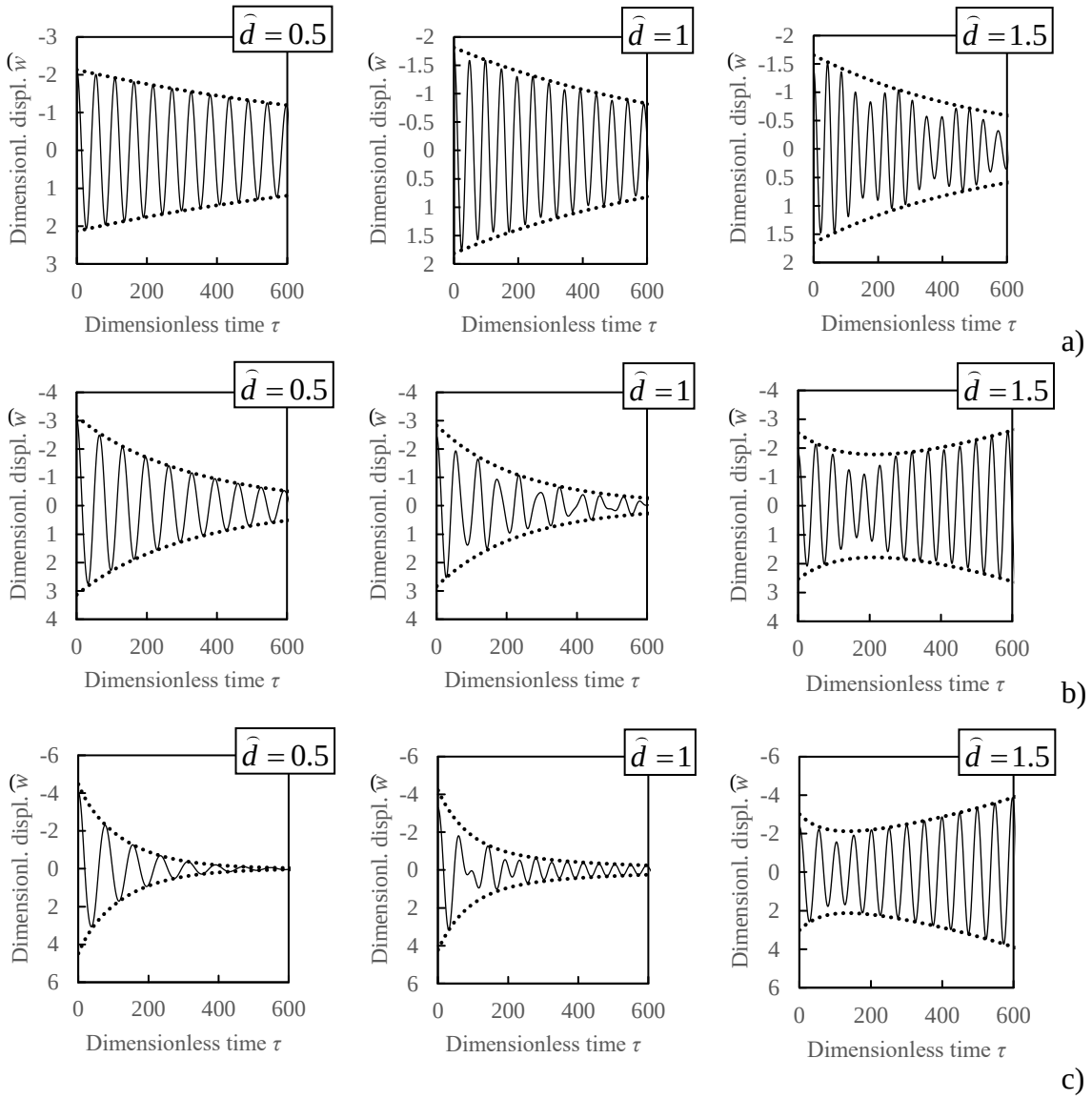

Figure 11: Unsteady harmonic part of vibrations for $\eta_M = 70$, $\eta_b = 0.05$, and $\widehat{d} = 0.5:0.5:1.5$: a) $\alpha = 0.5$; b) $\alpha = 0.8$; c) $\alpha = 0.9$ (black dotted lines indicate function envelopes).

It can be concluded that the decrease in the amplitudes is slower for a higher η_M. The instability is clearly identified in the final graphs Figures 11b) and c).

4.4 Onset of instability – one versus two moving masses

This section demonstrates the method to determine the onset of instability in a general manner. For such an analysis, it suffices to assume that there exists an induced frequency with a very low but negative imaginary part. Subsequently, it is possible to repeat the analysis for the same but positive value to confirm that the results obtained are practically unchanged, and therefore, the crossing of the imaginary axis has been detected correctly. Given the desired frequency, the target *K*-function value can be obtained from the characteristic equation. Thereafter, for a particular value of α, and in the case of two masses, for a particular $\hat{d}$ and η_b, the real part of the induced frequency and η_M can be solved by a simple integrative procedure. In this procedure, the two real unknowns are obtained from two equations by comparing the real and imaginary parts of the target and calculated *K*-function. The exact solution can be obtained by introducing the roots analytically, in the form presented in [37]; however, the analytical expression is rather complicated for use in a semi-analytical estimate.

In Figure 12, the damped case with $\eta_b = 0.05$ one moving mass is compared to two moving masses separated by $\hat{d} = 1 : 0.25 : 2$.

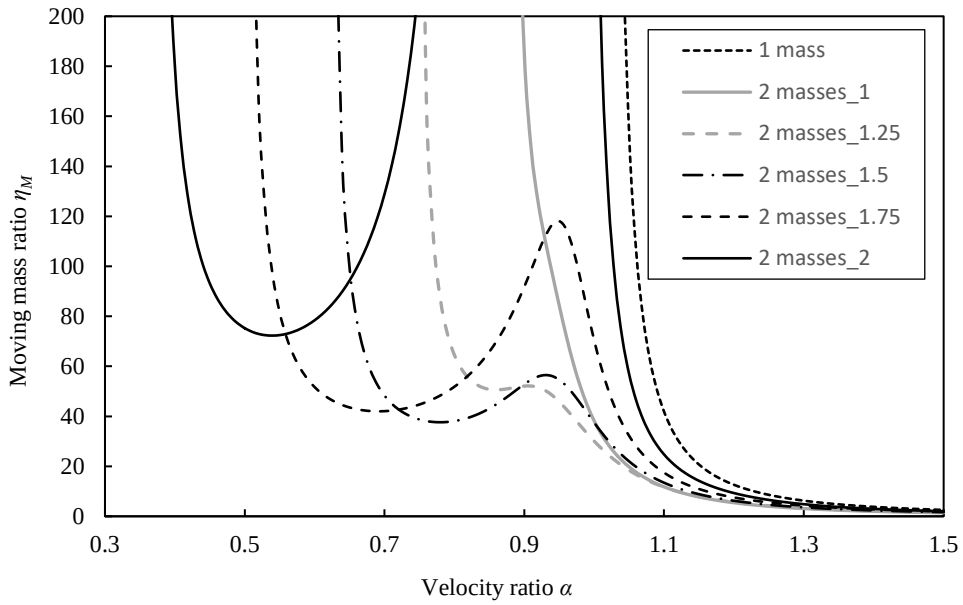

Figure 12: Velocity at onset of instability for one and two moving masses as function of η_M for $\eta_b = 0.05$ and $\hat{d} = 0.5 : 0.5 : 1.5$.

According to Figure 12, the damping always shifts the onset of instability to supercritical velocities for one moving mass. Although this conclusion was also presented in [22], the new

finding in this paper is that this is not true for additional moving masses. All presented curves cross the limit of $\alpha = 1$.

5. Conclusions

In this study, the new form of semi-analytical results to characterize the moving mass problem on infinite beams from [35-37] has been extended to account for the dynamic interaction between two proximate moving masses. The objective of this analysis was to demonstrate that result superposition is generally impossible unless the masses are far apart from one another. The other objective was to confirm that the dynamic interaction can alter the conditions for instability of one moving mass, which also subsequently indicates that superposition should not be used.

Preliminary results, available in [39], concluded that for a small distance between masses, these masses could be replaced by a single mass, and for a greater distance of the order $\hat{d} = 4.45$, superposition can be used. These conclusions were drawn based on analyses restricted to one velocity ratio $\alpha = 0.344$. Moreover, only a short period was examined, in which the effect of amplitude variation was not noticeable.

As in previous works, the new form of semi-analytical results was derived with the help of integral transforms and contour integration. The final closed-form formula for the full deflection shapes of the beam has been presented in the form of the sum of several terms. A specific designation is used because the transient part of the solution is separated into the unsteady harmonic and truly transient part. This separation is not related to the initial conditions but reflects the dominant part of the transient solution that can be expressed analytically using numerically obtained mass-induced frequencies, the number of which is finite. As this part is harmonic, it is referred to as the unsteady harmonic part. The other term, the mass-induced frequency, is distinguished from the natural frequencies because these frequencies are induced by the moving mass, and they involve not only the system but also the dynamic interaction resulting from the mass motion. The truly transient part, used for one additional part of the transient vibration, is generally negligible and is determined numerically. Another factor is the usual steady-state vibration. It was confirmed that the same procedure can be followed for one moving mass; however, the characteristic equation is more complicated, and the number of induced frequencies is higher than the one moving mass case. The role of the truly transient vibrations remains unchanged compared to the case of one moving mass, and the purpose is to adjust the initial conditions to the harmonic solution; their importance is temporary. The importance of the truly transient vibrations can be evaluated by the difference at zero time, and it is therefore not affected by damping or other factors.

The main limitation of the analyses presented in this paper is the assumption of continuous contact between the mass and the beam, but this is a common approach in similar works.

Nevertheless, if the moving force is sufficiently large, contact loss is not likely to occur. Other limitations relate to factors, such as the assumptions of uniform movement and a homogeneous structure with linear properties.

The main conclusions from this paper are as follows:

(i) In the undamped case, instability occurs exactly at the critical velocity, as for that of one moving mass.

(ii) In the undamped case, the frequency lines are cut in the subcritical velocity range when the real part reaches the limiting frequency q_{lm}.

(iii) In the undamped case, each induced frequency appears with all four sign combinations of the real and imaginary parts in the supercritical velocity range.

(iv) In the damped case, the frequency lines are cut when the imaginary part reaches the damping ratio η_b.

(v) In the subcritical velocity range, two pairs of frequencies exist for a lower α, and only one exists for a higher α. The lower frequency pair is always embedded between the limiting cases of the single and doubled mass. A smaller distance between the masses results in the frequency line being closer to that of the doubled mass. A greater distance between the masses results in the frequency line being closer to that of the single mass.

(vi) The higher frequency pair always lies outside the region specified in (v). In the absence of damping, the corresponding frequency line is cut by the first branch of the limiting frequency q_{lm}. A lower η_M or $\hat{d}$ results in a lower α when this occurs. In the damped case, the corresponding frequency line is also usually cut when the imaginary part reaches η_b, but no general conclusions can be drawn in such a case.

(vii) The higher frequency pair in the subcritical velocity range can significantly vary the amplitudes of the unsteady harmonic vibration.

(viii) In general, result superposition is not possible unless the masses are far apart, with a distance of at least $\hat{d} = 4.5$, which is the highest value considered in this study. Furthermore, substitution by one doubled mass is not possible in the full subcritical velocity range, even for $\hat{d} = 0.5$, which is the lowest value considered in this study.

(ix) In general, concerning the cases analyzed, the agreement between the full and harmonic solutions is excellent. The differences increase with a decreasing η_M in the vicinity of α_C and with an increasing $\hat{d}$ up to a particular limit, following which the agreement is recovered. For a large distance between masses, superposition would be possible, and, therefore, the conclusion relating to a single mass movement should be considered, where the aggravating factors are only the first two mentioned.

(x) In the damped case, damping can act in the opposite sense and shift the onset of instability into the subcritical range.

(xi) The critical distance between moving masses, defined as the distance for which the imaginary part of one of the induced frequencies is the lowest, is practically constant and only smoothly dependent on the damping: the dimensionless value changes smoothly from 1.25 to 1.05 within the damping range of $\eta_b = 0.04 : 0.01 : 0.99$.

(xii) As an example: at $\alpha = 0.99$ with $\eta_b = 0.05$ and $\widehat{d} = 1.25$, instability occurs for $\eta_M \geq 21.9$; at $\alpha = 0.99$ with $\eta_b = 0.1$ and $\widehat{d} = 1.2$, instability occurs for $\eta_M \geq 36.4$.

Points (ix) to (xii) constitute a warning that the analysis of transient vibrations is critical in the dynamic interaction of moving objects, and its omission could lead to overlooking the instability cases in situations when they are not expected.

It could be argued that the separation into the unsteady harmonic and truly transient parts is not necessary and that the complete solution can be obtained directly by numerical integration. This is not entirely true because full numerical integration is quite sensitive to numerical errors, particularly for longer times when it is difficult to maintain acceptable accuracy. However, most importantly, without careful analysis of the induced frequencies, several instability cases would remain uncovered.

Acknowledgements

This work was supported by the Portuguese Foundation for Science and Technology (FCT), through IDMEC, under LAETA, project UIDB/50022/2020.

References

[1] Z. Dimitrovová, “Semi-analytical approaches to vibrations induced by moving loads with the focus on the critical velocity and instability of the moving system”, pp. 97-152, in Ground Vibration from High Speed Railways, V.V. Krylov (Ed), ICE Publishing, Thomas Telford Ltd. ISBN: 9780727763792.

[2] L. Frýba, Vibration of solids and structures under moving loads, Research Institute of Transport, Prague (1972), 3rd edition, Thomas Telford, London, 1999.

[3] D. Basu, N.S.V. Kameswara Rao, Analytical solutions for Euler-Bernoulli beam on visco-elastic foundation subjected to moving load. *International Journal for Numerical Analytical Methods in Geomechanics*, **37**, 945–960, 2013.

[4] D. Froio, E. Rizzi, F.M.F. Simões, A.P. Da Costa, Universal analytical solution of the steady-state response of an infinite beam on a Pasternak elastic foundation under moving load, *International Journal of Solids and Structures*, **132–133,** 245–263, 2018.

[5] H.H. Jeffcott, On the vibrations of beams under the action of moving loads, *Philosophical Magazine*, Series 7, **8**(48), 66–97, 1929.

[6] J.E. Akin, M. Mofid, Numerical solution for response of beams with moving mass, *ASCE Journal of Structural Engineering*, **115**, 120–31, 1989.

[7] C.J. Bowe, T.P. Mullarkey, Unsprung wheel-beam interactions using modal and finite element models, *Advances in Engineering Software*, **39**, 911–922, 2008.

[8] M.A. Foda, Z. Abduljabbar, A dynamic green function formulation for the response of a beam structure to a moving mass, *Journal of Sound and Vibration*, **240**(5), 962–970, 1998.

[9] K. Kiani, A. Nikkhoo, B. Mehri, Prediction capabilities of classical and shear deformable beam models excited by a moving mass, *Journal of Sound and Vibration*, **320**(3), 632–648, 2009.

[10] D. Roshandel, M. Mofid, A. Ghannadiasl, Modal analysis of the dynamic response of Timoshenko beam under moving mass, *Scientia Iranica A* **22(**2), 331-344, 2015.

[11] F.R. Rofooei, A. Nikkhoo, Dynamic behavior and modal control of Euler-Bernoulli beams under moving mass, *Journal of Applied Mathematics*, **1**(1). 2008.

[12] R. Zarfam, A.R. Khaloo, A. Nikkhoo, On the response spectrum of Euler–Bernoulli beams with a moving mass and horizontal support excitation, *Mechanics Research Communications*, **47**, 77– 83. 2013.

[13] H.P, Lee, Transverse vibration of a Timoshenko beam acted upon by an accelerating mass, *Applied Acoustics* **47**(4), 319–330, 1996.

[14] G. Chen, L. Qian, Q. Yin, Dynamic analysis of a Timoshenko beam subjected to an accelerating mass using spectral element method, *Shock and Vibration*, Article ID 768209, 12 pages, 2014.

[15] I. Esen, Dynamic response of a functionally graded Timoshenko beam on two-parameter elastic foundations due to a variable velocity moving mass, *International Journal of Mechanical Sciences*, **153–154**, 21–35, 2019.

[16] S.A.Q. Siddiqui, M.F. Golnaraghi, G.R., Heppler, Large free vibrations of a beam carrying a moving mass, International Journal of Non-Linear Mechanics, 38, 1481-1493, 2003.

[17] A., Jahangiri, N.K.A., Attari, A., Nikkhoo, Z. Waezi, Nonlinear dynamic response of an Euler–Bernoulli beam under a moving mass–spring with large oscillations, *Archive of Applied Mechanics*, **90**, 1135–1156, 2020.

[18] D.G. Duffy, The response of an infinite railroad track to a moving, vibrating mass. *Journal of Applied Mechanics*, **57**(1), 66-73, 1990.

[19] S. Mackertich, The response of an elastically supported infinite Timoshenko beam to a moving vibrating mass, *Journal of the Acoustical Society of America*, **101**(1), 337-340, 1997.

[20] C.G. Koh, J.S.Y. Ong, D.K.H. Chua, J. Feng, Moving element method for train-track dynamics, International Journal for Numerical Methods in Engineering, 56, 1549-1567, 2003.

[21] H. Ouyang, Moving-load dynamic problems: A tutorial (with a brief overview), *Mechanical Systems and Signal Processing*, 25, 2039–2060, 2011.

[22] A.V. Metrikine, H.A. Dieterman, Instability of vibrations of a mass moving uniformly along an axially compressed beam on a visco-elastic foundation, *Journal of Sound and Vibration*, **201**, 567–576, 1997.

[23] A.V Metrikine, S.N. Verichev, Instability of vibrations of a moving two-mass oscillator on a flexibly supported Timoshenko beam, *Archive of Applied Mechanics*, **71,** 613-624, 2001.

[24] T. Mazilu, Interaction between a moving two-mass oscillator and an infinite homogeneous structure: Green's functions method, *Archive of Applied Mechanics*, **80**, 909-927, 2010.

[25] T. Mazilu,·M. Dumitriu, C. Tudorache, Instability of an oscillator moving along a Timoshenko beam on viscoelastic foundation, *Nonlinear Dynamics*, **67**, 1273–1293, 2012.

[26] V. Stojanović, P. Kozić, M.D. Petković, Dynamic instability and critical velocity of a mass moving uniformly along a stabilized infinity beam, *International Journal of Solids and Structures*, **108**, 164 ‑ 174, 2017.

[27] H.D. Nelson, R.A. Conover, Dynamic stability of a beam carrying moving masses, *Journal of Applied Mechanics, Transactions of the ASME*, **38**, 1003- 1006, 1971.

[28] G.A. Benedetti, Dynamic stability of a beam loaded by a sequence of moving mass particles, *Journal of Applied Mechanics, Transactions of the ASME*, **41**, 1069- 1071, 1974.

[29] S. Mackertich, Dynamic response of a supported beam to oscillatory moving masses, *Journal of Vibration and Control*, **9**(9), 1083–1091, 2003.

[30] B. Yang, H. Gao, S. Liu, Vibrations of a Multi-Span Beam Structure Carrying Many Moving Oscillators, *International Journal of Structural Stability and Dynamics*, **18**(10), 1850125, 2018.

[31] T. Mazilu, Instability of a train of oscillators moving along a beam on a viscoelastic foundation, *Journal of Sound and Vibration*, **332**, 4597–4619, 2013.

[32] V. Stojanović, M.D. Petković, J. Deng, Stability and vibrations of an overcritical speed moving multiple discrete oscillators along an infinite continuous structure, *European Journal of Mechanics - A/Solids*, **75**, 367–380, 2019.

[33] S. Roy, G. Chakraborty, A. DasGupta, Coupled dynamics of a viscoelastically supported infinite string and a number of discrete mechanical systems moving with uniform speed, *Journal of Sound and Vibration*, **415**, 184–209, 2018.

[34] A.S.E. Nassef, M.M. Nassar, M.M. EL-Refaee, Dynamic response of Timoshenko beam resting on nonlinear Pasternak foundation carrying sprung masses, *Iranian Journal of Science and Technology, Transactions of Mechanical Engineering*, **43**, 419–426, 2019.

[35] Z. Dimitrovová, New semi-analytical solution for a uniformly moving mass on a beam on a two-parameter visco-elastic foundation, *International Journal of Mechanical Sciences*, **127**, 142–162, 2017.

[36] Z. Dimitrovová, Complete semi-analytical solution for a uniformly moving mass on a beam on a two-parameter visco-elastic foundation with non-homogeneous initial conditions, *International Journal of Mechanical Sciences*, **144**, 283-311, 2018.

[37] Z. Dimitrovová, Semi-analytical solution for a problem of a uniformly moving oscillator on an infinite beam on a two-parameter visco-elastic foundation, *Journal of Sound and Vibration*, **438**, 257-290, 2019.

[38] Z. Dimitrovová, Semi-analytical analysis of vibrations induced by a mass traversing a beam supported by a finite depth foundation with simplified shear resistance, *Meccanica,* **55**(12), pp. 2353–2389, 2020.

[39] Z. Dimitrovová, Analysis of vibrations induced by an oscillator traversing a beam supported by a finite depth foundation with simplified shear resistance, XI International Conference on Structural Dynamics (EURODYN 2020), 23-26/11/2020, Athens, Greece. Proceedings of the International Conference on Structural Dynamic, EURODYN, 2020, 2, pp. 2658–2666, *EASD Proceedia*

[40] M.E. Hassanabadi, N.K.A. Attari, A. Nikkhoo, M. Baranadan, An optimum modal superposition approach in the computation of moving mass induced vibrations of a

distributed parameter system, *Proc IMechE Part C: Journal of Mechanical Engineering Science*, **229**(6), 1015–1028, 2015.

Appendix

In this Appendix, deflections of the rear contact point are summarized for some of the analyzed cases. For the sake of comparison, solutions obtained by superposition of results related to one single mass are also added. In addition, solutions related to one doubled mass are included, but only when the distance between masses is low. It is demonstrated that neither results superposition, nor replacement by one doubled mass can lead to acceptable approximations.

Analyses of the importance of the truly transient vibrations are included alongside with the results validation. Full solution is obtained on finite beams, nevertheless, same results could be obtained by adding the truly transient part (calculated numerically) to the harmonic solution. As proven in previous works [35-38], such results are equivalent.

Undamped cases are summarized in Figures A.1-2. Only cases with $\eta_M = 40$, $\alpha = 0.5$ or $\alpha = 0.9$, and $\widehat{d} = 0.5 : 0.5 : 4.5$ are shown for illustration.

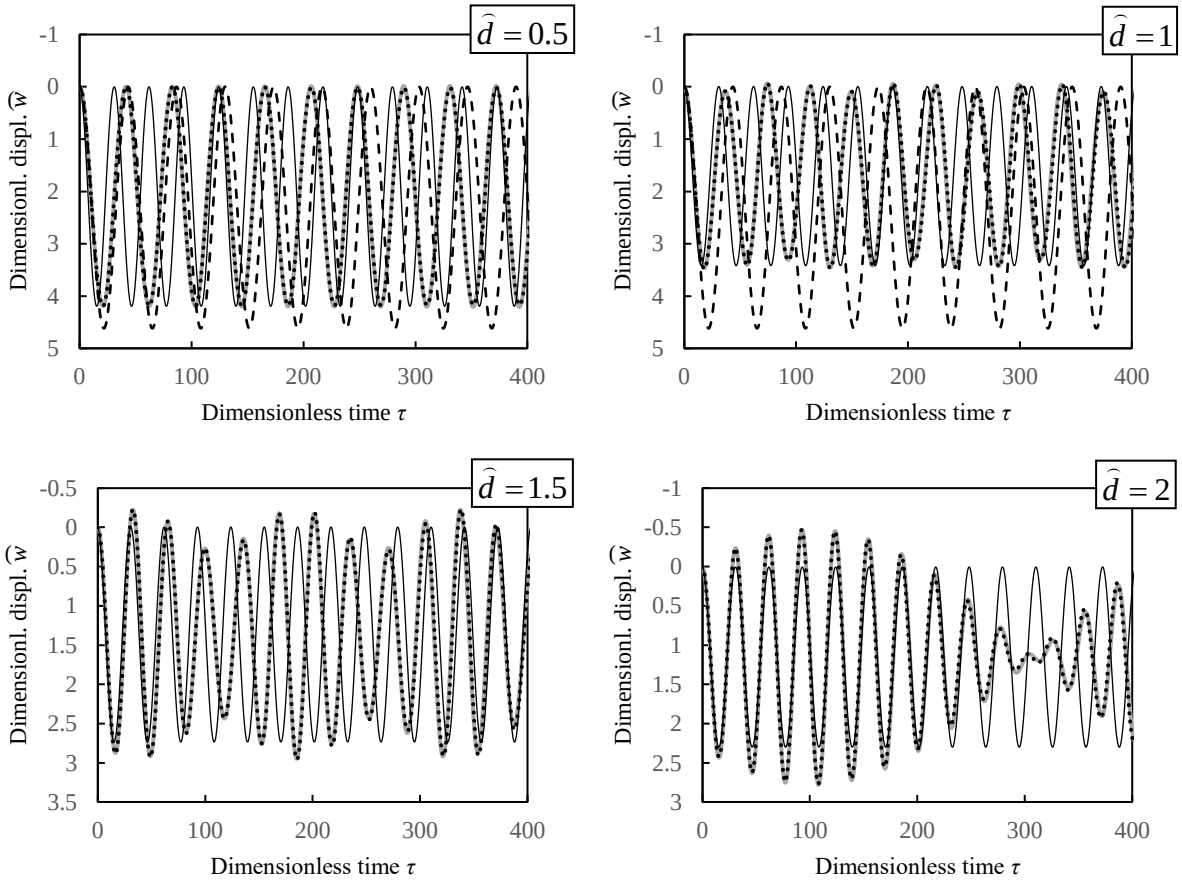

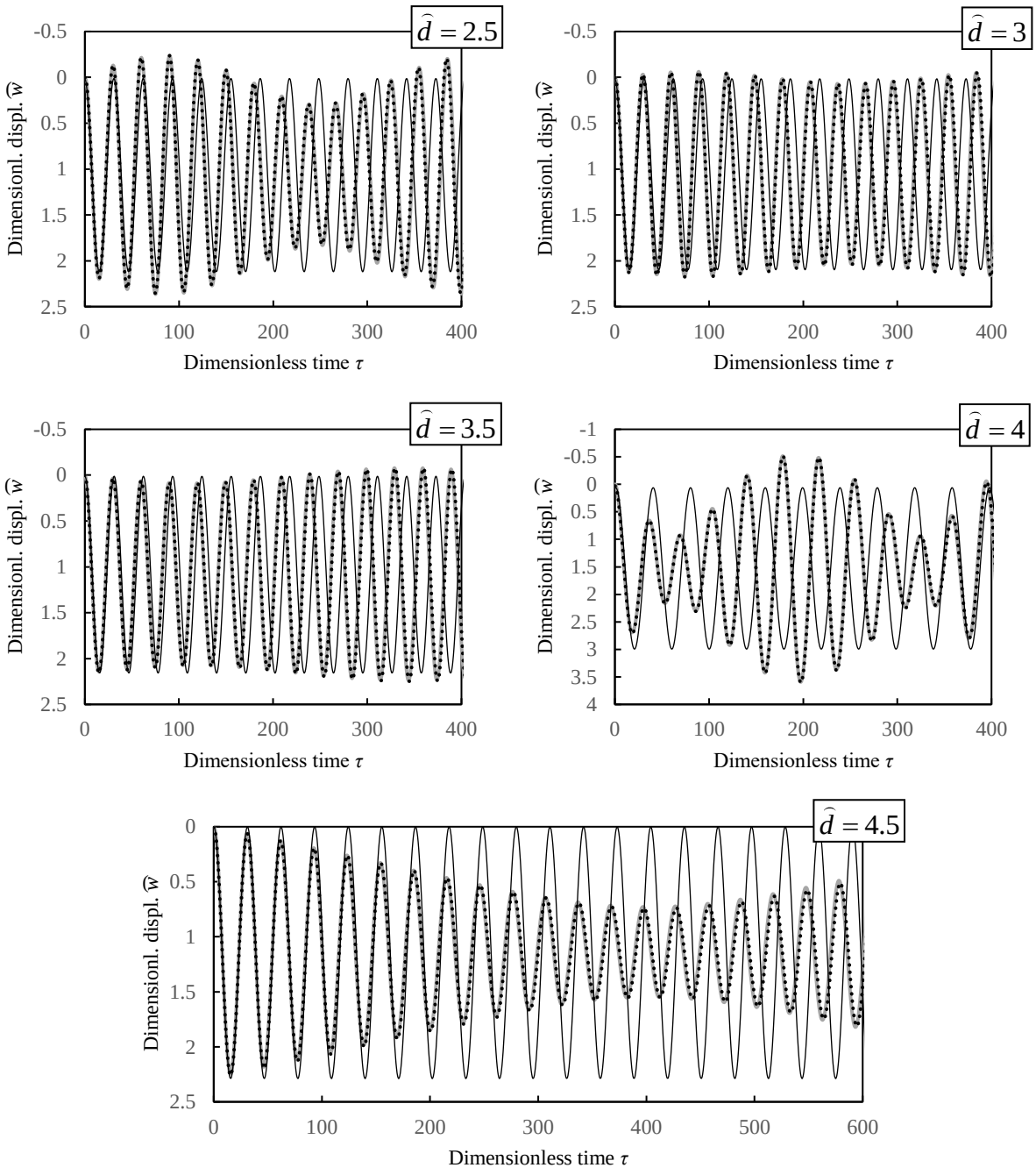

Figure A.1: Vibration comparison for $\eta_M = 40$, $\alpha = 0.5$ and $\hat{d} = 0.5 : 0.5 : 4.5$ (grey - full solution obtained on finite beam, dotted - harmonic solution, black – superposition, dashed – doubled mass, omitted for $\hat{d} = 1.5$ and larger due to large discrepancies).

It can be concluded from Figure A.1 that the agreement between the full and harmonic solutions is excellent and neither superposition nor doubled mass stand for some acceptable approximation.

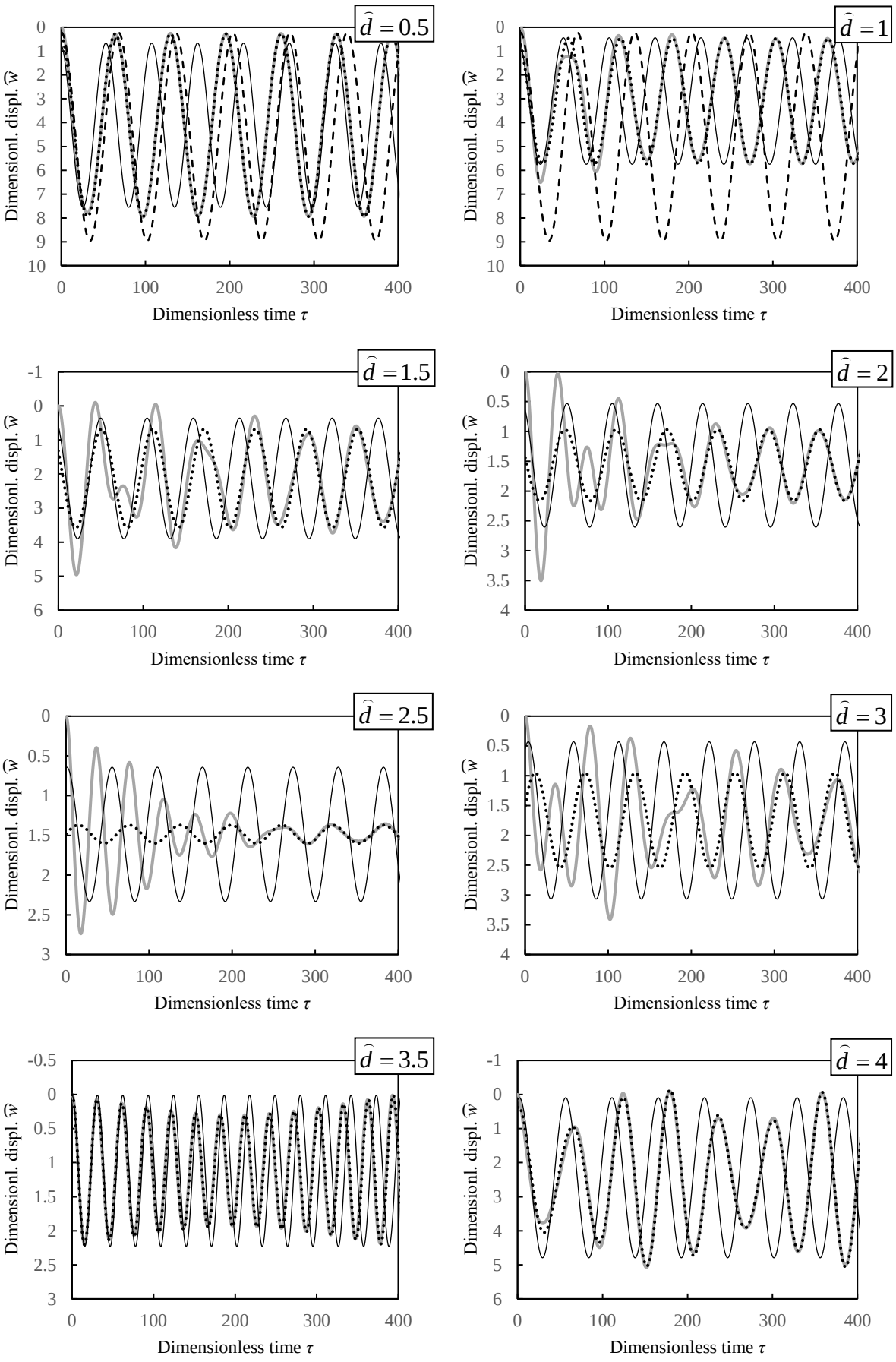
$\hat{d} = 0.5$
$\hat{d} = 1$
$\hat{d} = 1.5$
$\hat{d} = 2$
$\hat{d} = 2.5$
$\hat{d} = 3$
$\hat{d} = 3.5$
$\hat{d} = 4$
Dimensionl. displ. $\hat{w}$
Dimensionless time τ

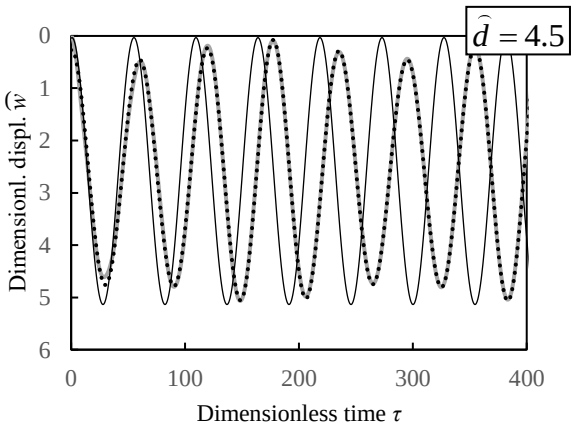

Figure A.2: Vibration comparison for $\eta_M = 40$, $\alpha = 0.9$ and $\hat{d} = 0.5 : 0.5 : 4.5$ (grey - full solution obtained on finite beam, dotted - harmonic solution, black – superposition, dashed – doubled mass, omitted for $\hat{d} = 1.5$ and larger due to large discrepancies).

Besides previous conclusions, it is shown in Figure A.2 that there is a noticeable disagreement between the full and harmonic solutions starting from $\hat{d} = 1.5$, however, the agreement is recovered starting from $\hat{d} = 3.5$.

Figures A.1-2 clearly evidence that for low distances between mases the solution obtained for doubled mass does not stand for a good approximation, because the amplitude is noticeably higher and does not exhibit any form of variation. The difference in frequency is also visible. It is also evidenced that even for $\hat{d} = 4.5$, the approximation by results superposition is not yet acceptable, due to the same reasons as mentioned above, i.e., lack of amplitudes variation and discrepancies in frequencies.

In the damped cases some of the previous conclusions cannot be clearly visible, because in several cases damping attenuates the transient vibrations very quickly. Nevertheless, as already mentioned, instability can occur in subcritical velocity range, and this can only be detected by analysis of the transient vibrations.

In conformity with previous cases, full and harmonic solutions and compared with results obtained by superposition in Figures A.3–5. For distances between masses below $\hat{d} = 1.5$, also solution for doubled mass is added.

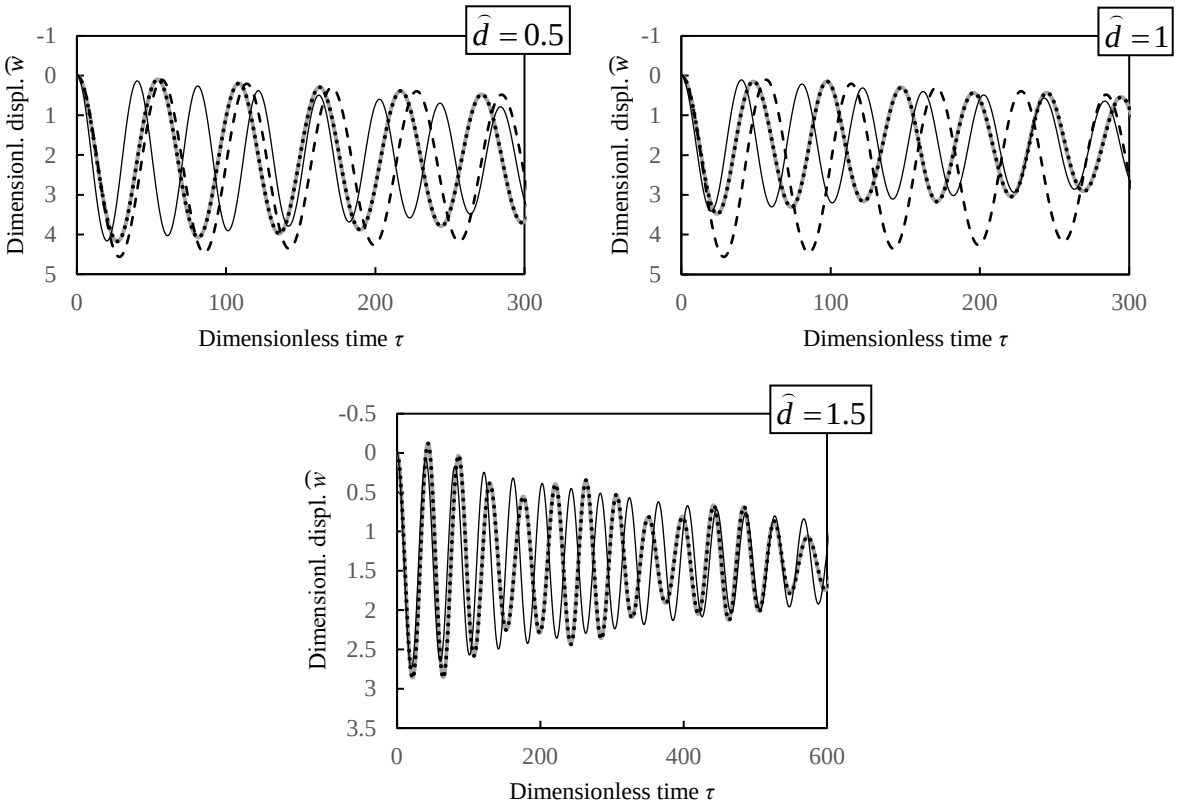

Figure A.3: Vibration comparison for $\eta_M = 70$, $\alpha = 0.5$, $\eta_b = 0.05$, $\hat{d} = 0.5 : 0.5 : 1.5$ (grey - full solution obtained on finite beam, dotted - harmonic solution, black – superposition, dashed – doubled mass, omitted for $\hat{d} = 1.5$ and larger due to large discrepancies).

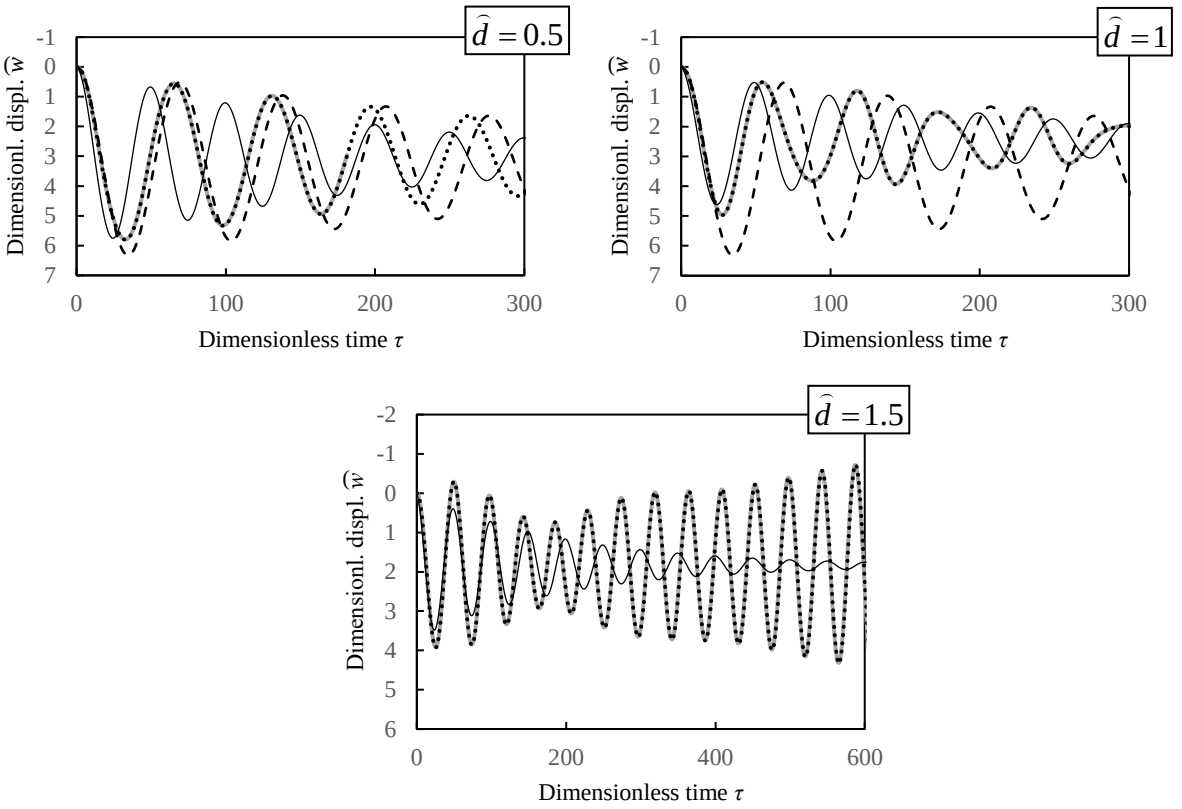

Figure A.4: Vibration comparison for $\eta_M = 70$, $\alpha = 0.8$, $\eta_b = 0.05$, $\hat{d} = 0.5:0.5:1.5$ (grey - full solution obtained on finite beam, dotted - harmonic solution, black – superposition, dashed – doubled mass, omitted for $\hat{d} = 1.5$ and larger due to large discrepancies).

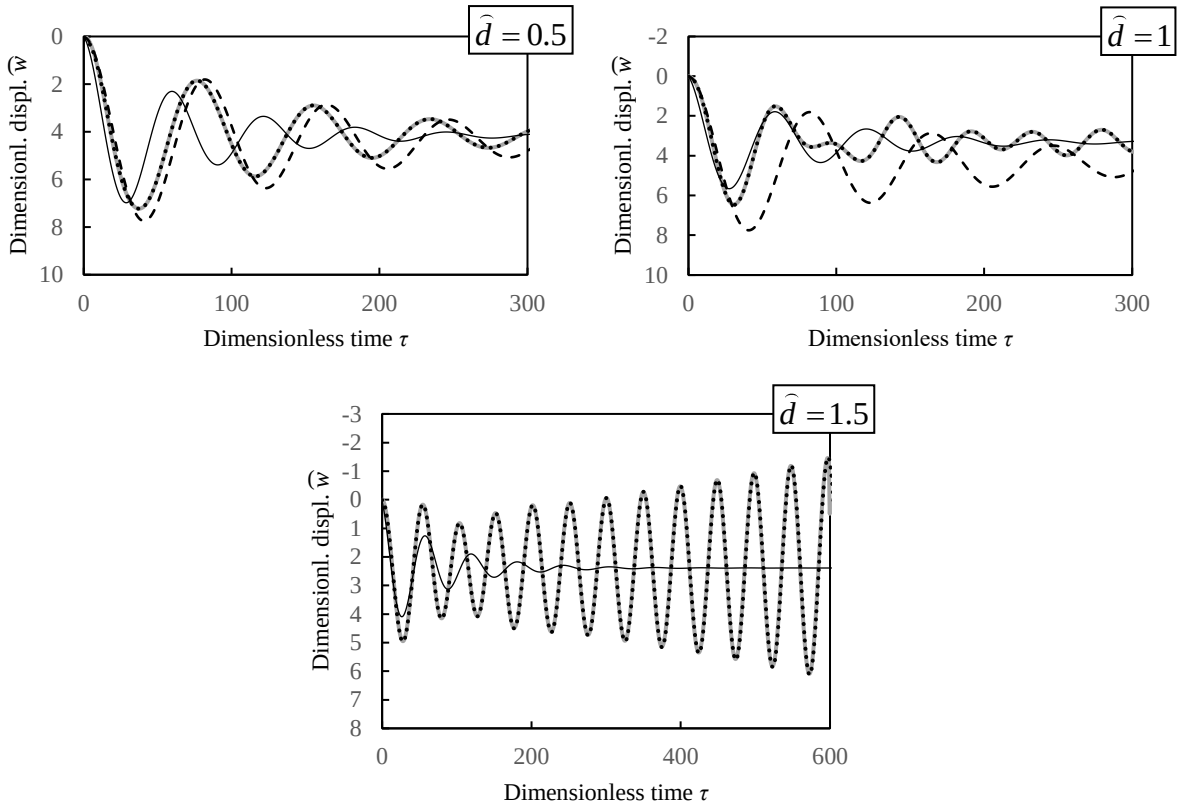

Figure A.5: Vibration comparison for $\eta_M = 70$, $\alpha = 0.9$, $\eta_b = 0.05$, $\hat{d} = 0.5:0.5:1.5$ (grey - full solution obtained on finite beam, dotted - harmonic solution, black – superposition, dashed – doubled mass, omitted for $\hat{d} = 1.5$ and larger due to large discrepancies).

Unstable cases are clearly identified and validated in last graphs of Figures A.4–5. All cases show excellent agreement between the full and harmonic solutions, as it is usual for higher η_M. It is also clear that neither superposition nor doubled mass represent some acceptable solution, concerning the cases analyzed.